16

Formulation of flexible elements

This chapter deals with the formulations of flexible elements such as flexible joints, cables, beams, and plates and shells, which are presented in sections 16.1, 16.2, 16.3, and 16.4, respectively. In all cases, geometrically exact formulations are derived, *i.e.*, the displacements and rotations of the elements are arbitrarily large, although strain components are assumed remain small, a feature that significantly simplifies the governing equations of motion of these structural components.

16.1 Formulation of flexible joints

Flexible joints, sometimes called bushing elements or force elements, are found in all multibody dynamics codes. In their simplest form, flexible joints consist of sets of three linear and three torsional springs placed between two nodes of a multibody system. For infinitesimal deformations, the selection of the lumped spring constants is an easy task, which can be based on a numerical simulation of the joint or on experimental measurements.

If the joint undergoes finite deformations, identification of its stiffness characteristics is not so simple, specially if the joint is itself a complex system. When finite deformations occur, the definition of deformation measures becomes a critical issue. Indeed, for finite deformation, the observed nonlinear behavior of materials is partly due to material characteristics, and partly due to kinematics.

This section focuses on the determination of the proper finite deformation measures for elastic bodies of *finite dimension*. In contrast, classical strain measures, such as the Green-Lagrange strains presented in section 15.3.4, among many others, characterize finite deformations of *infinitesimal elements of a body*. It is argued that proper finite deformation measures must be of a tensorial nature, *i.e.*, must present specific invariance characteristics. This requirement is satisfied if and only if deformation measures are parallel to the eigenvector of the motion tensor.

Anand [288, 289] has shown that the classical strain energy function for infinitesimal isotropic elasticity is in good agreement with experiment for a wide class of materials for moderately large deformations, provided the infinitesimal strain measure

O. A. Bauchau, *Flexible Multibody Dynamics,*
DOI 10.1007/978-94-007-0335-3_16

used in the strain energy function is replaced by the Hencky or logarithmic measure of finite strain. This means that the behavior of materials for moderate deformations can be captured accurately using linear constitutive laws, but replacing the infinitesimal strain measures by finite deformation measures that are nonlinear functions of the displacements.

These nonlinear deformation measures capture the observed nonlinear behavior associated with the nonlinear kinematics of the problem. Degener *et al.* [290] also reported similar findings for the torsional behavior of beams subjected to large axial elongation.

Much attention has been devoted to the problem of synthesizing accurate constitutive properties for the modeling of flexible bushings presenting complex, time-dependent rheological behavior [291, 292]. It is worth stressing, however, that the literature seldom addresses three-dimensional joint deformations.

Much like multibody codes, most finite element codes also support the modeling of lumped structural elements. While linear analysis is easily implemented, problems are encountered when dealing with finite displacements and rotations, as pointed out by Masarati and Morandini [293]. Structural analysis codes, either specifically intended for multibody dynamics analysis, like MSC/ADAMS, or for nonlinear finite element codes with multibody capabilities, like Abaqus/Standard, allow arbitrarily large absolute displacements and rotations of the nodes and correctly describe their rigid-body motion. When lumped deformable joints are used, relative displacements and rotations are often required to remain moderate, although not necessarily infinitesimal.

Such restrictions occur when using the FIELD element of MSC/ADAMS, a linear element that implements an orthotropic torsional spring based on a constant, orthotropic constitutive matrix [294]. Similarly, the JOINTC element implemented in Abaqus/Standard, describes the interaction between two nodes when the second node can "displace and rotate slightly with respect to the first node [295]," because its formulation is based on an approximate relative rotation measure.

The formulations and implementations of flexible joints available in research and commercial codes do not appear to allow arbitrarily large relative displacements and rotations. Moreover, in many cases, the ordering sequence of the nodes connected to the joint matters, because the behavior of the flexible joint is biased towards one of the nodes. This problem is known to experienced analysts using these codes. To the authors' knowledge, these facts are rarely acknowledged in the literature. It appears that little effort has been devoted to the elimination of these shortcomings from the formulations found in research and commercially available codes, although the predictions of these codes might be unexpected.

This section presents families of finite deformation measures that can be used to characterize the deformation of flexible joints. These deformation measures are closely related to the tensorial parameterization motion developed in chapter 14. Because they are of a tensorial nature, these deformation measures are intrinsic and invariant. Furthermore, it will be shown that using these strain measures in combination with the linear constitutive laws of the joint enable the accurate prediction of joint behavior under moderate deformation.

16.1.1 Flexible joint configuration

Figure 16.1 shows a flexible joint in its reference and deformed configurations. It consists of a three-dimensional elastic body of finite dimension and of two rigid bodies, called handle k and handle ℓ, that are rigidly connected to the elastic body. In the reference configuration, the configuration of the handles is defined by frame $\mathcal{F}_0 = \left[\mathbf{K} = \mathbf{L}, \mathcal{B}_0 = (\bar{b}_{01}, \bar{b}_{02}, \bar{b}_{03})\right]$, where $\mathcal{B}_0$ forms an orthonormal basis. Points **K** and **L** are material points of handles k and ℓ, respectively, with coincident geometric locations.

In the deformed configuration, the two handles move to new positions and the elastic body deforms. Points **K** and **L** are now at distinct locations; the relative displacement vector of point **L** with respect to point **K** is denoted $\underline{u}$. The configurations of the two handles are now distinct and two distinct frames, $\mathcal{F}^k = \left[\mathbf{K}, \mathcal{B}^k = (\bar{b}_1^k, \bar{b}_2^k, \bar{b}_3^k)\right]$ and $\mathcal{F}^\ell = \left[\mathbf{L}, \mathcal{B}^\ell = (\bar{b}_1^\ell, \bar{b}_2^\ell, \bar{b}_3^\ell)\right]$, define the configurations of handle k and ℓ, respectively. The relative rotation tensor of basis $\mathcal{B}^\ell$ with respect to basis $\mathcal{B}^k$ is denoted $\underline{\underline{R}}$.

The deformation of the flexible joint stems from applied forces and moments. At point **K**, the applied force and moment vectors are denoted $\underline{F}_k$ and $\underline{M}_k$, respectively; the corresponding quantities applied at point **L** are denoted $\underline{F}_\ell$ and $\underline{M}_\ell$, respectively. The loading applied to the flexible joint is defined in the following manner

$$\underline{\mathcal{A}}_k = \begin{Bmatrix} \underline{F}_k \\ \underline{M}_k \end{Bmatrix}, \quad \underline{\mathcal{A}}_\ell = \begin{Bmatrix} \underline{F}_\ell \\ \underline{M}_\ell \end{Bmatrix}, \tag{16.1}$$

where $\underline{\mathcal{A}}_k$ and $\underline{\mathcal{A}}_\ell$ denote the loads applied at points **K** and **L**, respectively. According to Newton's third law, these loads must be in equilibrium, *i.e.*,

$$\underline{\mathcal{A}}_k = -\begin{bmatrix} \underline{\underline{I}} & \underline{\underline{0}} \\ \underline{\tilde{u}} & \underline{\underline{I}} \end{bmatrix} \underline{\mathcal{A}}_\ell. \tag{16.2}$$

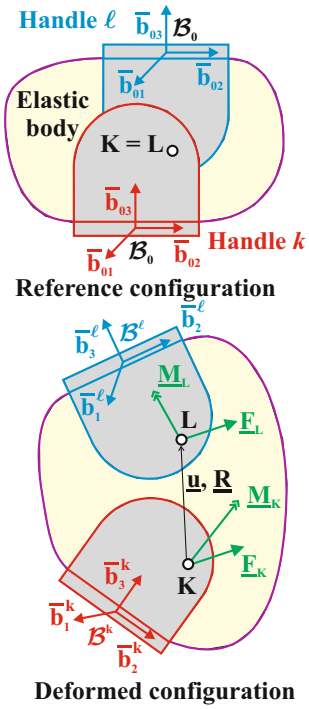

Fig. 16.1. Configuration of the flexible joint.

The joint is assumed to be massless, *i.e.*, inertial forces associated with its motion are neglected.

The state of deformation of the elastic body depends on the relative displacement and rotation of the two handles and is unaffected by rigid body motions. Consequently, it is possible to assume that handle k does not move, and the relative displacement and rotation of handle ℓ with respect to handle k then simply becomes its absolute motion, as illustrated in fig. 16.2. This configuration is denoted scenario ℓ. Of course, scenario k could also be defined in a similar manner if the location of handle ℓ is assumed to remain fixed in space.

Consider the differential displacement of point **L** shown in fig 16.2. The components of this differential displacement vector in bases $\mathcal{B}^k$ and $\mathcal{B}^\ell$ are $\mathrm{d}\underline{u}^+$ and $\underline{\underline{R}}^T\mathrm{d}\underline{u}^+$, respectively. The components of the differential rotation vector of handle ℓ are denoted $\underline{\mathrm{d}\psi}^+ = \mathrm{axial}(\mathrm{d}\underline{\underline{R}}\,\underline{\underline{R}}^T)$ and $\underline{\mathrm{d}\psi}^* = \mathrm{axial}(\underline{\underline{R}}^T\mathrm{d}\underline{\underline{R}}) = \underline{\underline{R}}^T\underline{\mathrm{d}\psi}^+$ when resolved in the same bases, respectively. The differential motion vector of point **L** is now defined as

$$\underline{\mathrm{d}\mathcal{U}}^*_\ell = \begin{Bmatrix} \underline{\underline{R}}^T\mathrm{d}\underline{u}^+ \\ \underline{\underline{R}}^T\underline{\mathrm{d}\psi}^+ \end{Bmatrix}. \tag{16.3}$$

Superscripts $(\cdot)^+$ and $(\cdot)^*$ indicate tensor components resolved in basis $\mathcal{B}^k$ and $\mathcal{B}^\ell$, respectively.

The differential motion of the point of handle ℓ that instantaneously coincides with the origin of reference frame $\mathcal{F}_0$, denoted $\underline{\mathrm{d}\mathcal{U}}^+_\ell$, is found from the following frame change operation

$$\begin{aligned}\underline{\mathrm{d}\mathcal{U}}^+_\ell &= \begin{Bmatrix} \mathrm{d}\underline{u}^+ + \widetilde{u}^+\underline{\mathrm{d}\psi}^+ \\ \underline{\mathrm{d}\psi}^+ \end{Bmatrix} \\ &= \underline{\underline{\mathcal{C}}}(\underline{u}^+, \underline{\underline{R}}^+)\underline{\mathrm{d}\mathcal{U}}^*_\ell,\end{aligned} \tag{16.4}$$

where $\underline{\underline{R}}^+ = \underline{\underline{R}}$.

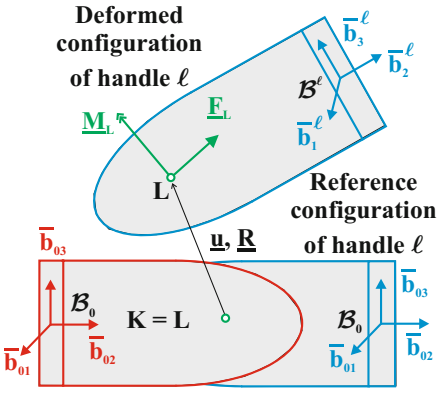

Fig. 16.2. Configuration of the flexible joint for scenario ℓ. For clarity of the figure, the elastic body is not shown.

The load externally applied at point **L**, denoted $\underline{\mathcal{A}}_\ell$, was defined in eq. (16.1). These applied force and moment vectors are now resolved in basis $\mathcal{B}^\ell$ to form $\underline{\mathcal{A}}^{*T}_\ell = \{\underline{F}^{*T}_\ell, \underline{M}^{*T}_\ell\}$. The following change of frame operation is now considered

$$\underline{\mathcal{A}}^+_\ell = \begin{Bmatrix} \underline{F}^+_\ell \\ \underline{M}^+_\ell + \widetilde{u}^+\underline{F}^+_\ell \end{Bmatrix} = \underline{\underline{\mathcal{C}}}^{-T}(\underline{u}^+, \underline{\underline{R}}^+)\underline{\mathcal{A}}^*_\ell. \tag{16.5}$$

Note the parallel between vector $\underline{\mathcal{A}}^+_\ell$ and the second Piola-Kirchhoff stress tensor [296]. Indeed, $\underline{\mathcal{A}}^+_\ell$ represents the true loads applied to handle ℓ in its deformed configuration, but transferred to the original location of their application point in the reference configuration. Loads $\underline{\mathcal{A}}^+_\ell$ and $\underline{\mathcal{A}}^*_\ell$ form a set of equipollent loads applied to handle ℓ. The change of frame operation described by eq. (16.5), expresses, in fact, a condition of equipollence.

16.1.2 Flexible joint differential work

The differential work, $\mathrm{d}W$, done by the forces applied to the joint is

$$\mathrm{d}W = \underline{F}^{+T}_\ell\mathrm{d}\underline{u}^+ + \underline{M}^{+T}_\ell\underline{\mathrm{d}\psi}^+ = \underline{\mathcal{A}}^{*T}_\ell\underline{\mathrm{d}\mathcal{U}}^*_\ell = \underline{\mathcal{A}}^{+T}_\ell\underline{\mathrm{d}\mathcal{U}}^+_\ell, \tag{16.6}$$

where the last two equalities follow from eqs. (5.57) and (5.61), respectively. Because handle k does not move, the forces and moments applied at point **K** do not work.

Let $\underline{\mathcal{E}}_\ell^+$ be a set of six generalized coordinates that uniquely define the configuration of handle ℓ, *i.e.*, a one-to-one mapping is assumed to exist between these generalized coordinates and the configuration of handle ℓ. It then follows that a one-to-one mapping must exist between the handle's differential motion and differentials of the generalized coordinates

$$\underline{\mathrm{d}\mathcal{U}}_\ell^* = \underline{\underline{\mathcal{H}}}^*(\underline{\mathcal{E}}_\ell^+)\mathrm{d}\underline{\mathcal{E}}_\ell^+, \quad \underline{\mathrm{d}\mathcal{U}}_\ell^+ = \underline{\underline{\mathcal{H}}}(\underline{\mathcal{E}}_\ell^+)\mathrm{d}\underline{\mathcal{E}}_\ell^+. \tag{16.7}$$

Matrix $\underline{\underline{\mathcal{H}}}(\underline{\mathcal{E}}_\ell^+)$ is the Jacobian matrix or tangent operator of the coordinate transformation.

The differential work done by the forces applied to the joint, eq. (16.6), now becomes

$$\mathrm{d}W = \underline{\mathcal{A}}_\ell^{*T}\underline{\underline{\mathcal{H}}}^*(\underline{\mathcal{E}}_\ell^+)\mathrm{d}\underline{\mathcal{E}}_\ell^+ = \underline{\mathcal{A}}_\ell^{+T}\underline{\underline{\mathcal{H}}}(\underline{\mathcal{E}}_\ell^+)\mathrm{d}\underline{\mathcal{E}}_\ell^+ = \underline{\mathcal{L}}_\ell^{+T}\mathrm{d}\underline{\mathcal{E}}_\ell^+, \tag{16.8}$$

where the generalized forces associated with the generalized coordinates are defined as

$$\underline{\mathcal{L}}_\ell^+ = \underline{\underline{\mathcal{H}}}^{*T}(\underline{\mathcal{E}}_\ell^+)\underline{\mathcal{A}}_\ell^* = \underline{\underline{\mathcal{H}}}^T(\underline{\mathcal{E}}_\ell^+)\underline{\mathcal{A}}_\ell^+. \tag{16.9}$$

It is now assumed that the flexible joint is made of an elastic material [285], which implies that the generalized forces can be derived from a potential, the strain energy of the joint, denoted A,

$$\underline{\mathcal{L}}_\ell^+ = \frac{\partial A(\underline{\mathcal{E}}_\ell^+)}{\partial \underline{\mathcal{E}}_\ell^+}. \tag{16.10}$$

The differential work now becomes

$$\mathrm{d}W = \mathrm{d}\underline{\mathcal{E}}_\ell^{+T}\frac{\partial A(\underline{\mathcal{E}}_\ell^+)}{\partial \underline{\mathcal{E}}_\ell^+} = \mathrm{d}(A), \tag{16.11}$$

and can be expressed as the differential of a scalar function, the strain energy.

The reasoning presented in this section could be repeated for scenario k. Because scenarios k and ℓ only differ by a rigid body motion, identical results should be obtained. In particular, the differential work for the two scenarios should be identical, leading to $\mathrm{d}W = \underline{\mathcal{A}}_\ell^{+T}\underline{\mathrm{d}\mathcal{U}}_\ell^+ = \underline{\mathcal{A}}_k^{+T}\underline{\mathrm{d}\mathcal{U}}_k^+$. Loading $\underline{\mathcal{A}}_\ell^+$ and $\underline{\mathcal{A}}_k^+$ are referred to the same point, the origin of frame $\mathcal{F}_0$, and expressed in the same basis, $\mathcal{B}_0$; Newton's first law then implies $\underline{\mathcal{A}}_\ell^+ + \underline{\mathcal{A}}_k^+ = 0$, leading to the intuitive result that

$$\underline{\mathrm{d}\mathcal{U}}_k^+ = -\underline{\mathrm{d}\mathcal{U}}_\ell^+. \tag{16.12}$$

16.1.3 The deformation measures

In the previous section, quantities $\underline{\mathcal{E}}_\ell^+$ were defined as "a set of generalized coordinates that uniquely define the configuration of handle ℓ," but were otherwise left

undefined. For scenario ℓ, the configuration of handle ℓ defines the deformation of the elastic body, and hence, these generalized coordinates are, in fact, deformation measures for the flexible joint. The following notation is introduced

$$\underline{\mathcal{E}}_\ell^+ = \begin{Bmatrix} \underline{\epsilon}^+ \\ \underline{\kappa}^+ \end{Bmatrix}. \tag{16.13}$$

The first three components of this array form the stretch vector, denoted $\underline{\epsilon}$, and the last three the wryness vector, denoted $\underline{\kappa}$. Both quantities are assumed to form first-order tensors.

Because the deformation measures uniquely define the configuration of handle ℓ relative to handle k, the motion tensor, $\underline{\underline{\mathcal{C}}}(\underline{u}, \underline{\underline{R}})$, can be expressed as $\underline{\underline{\mathcal{C}}} = \underline{\underline{\mathcal{C}}}(\underline{\mathcal{E}}_\ell^+)$. It follows that the deformation measures form a parameterization of the motion tensor. In general, the deformation measures are nonlinear functions of six quantities, the three components of the relative displacement vector, $\underline{u}$, and the three parameters that define the relative rotation tensor, $\underline{\underline{R}}$.

For instance, the stretch vector could be selected as the position vector of point **L**, $\underline{\epsilon}^+ = \underline{u}^+$; note that $\underline{\epsilon}^* = \underline{\underline{R}}^T \underline{\epsilon}^+$, as expected from the tensorial nature of the stretch vector. The Euler angles associated with rotation tensor $\underline{\underline{R}}$ form a valid set of generalized coordinates to characterize the angular motion of handle ℓ, but cannot be the components of the wryness vector because Euler angles do not form the components of a vector. Any vectorial parameterization of rotation, see section 13.4, is a suitable choice for the wryness vector.

16.1.4 Change of reference frame

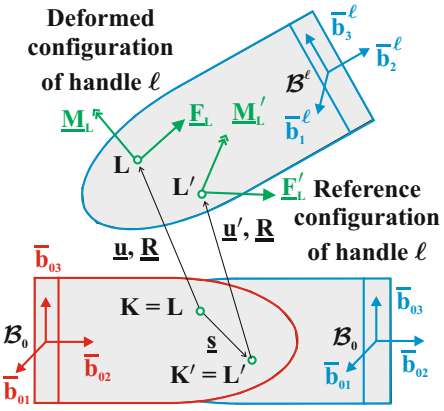

Fig. 16.3. Configuration of the flexible joint for scenario ℓ. For clarity of the figure, the elastic body is not shown.

The results derived in section 16.1.2 were based on the selection of an arbitrary reference frame, $\mathcal{F}_0$, defined by coincident reference points, **K** = **L**, which are material points of handles k and ℓ, respectively, and an orthonormal basis, $\mathcal{B}_0$. Another reference frame could have been selected, $\mathcal{F}'_0 = \left[\mathbf{K}' = \mathbf{L}', \mathcal{B}'_0 = (\bar{b}'_{01}, \bar{b}'_{02}, \bar{b}'_{03})\right]$; figure 16.3 shows the new reference points, $\mathbf{K}'$ = $\mathbf{L}'$, which are material points of handles k and ℓ, respectively. For clarity, the new basis, $\mathcal{B}'_0$, is not shown on the figure. The position vector of point $\mathbf{K}'$ with respect to point **K** is denoted $\underline{s}$ and the relative rotation tensor of basis $\mathcal{B}'_0$ with respect to basis $\mathcal{B}_0$ is denoted $\underline{\underline{S}}$. The motion tensor that brings frame to $\mathcal{F}_0$ to $\mathcal{F}'_0$ is denoted $\underline{\underline{\mathcal{C}}}'(\underline{s}, \underline{\underline{S}})$.

The development presented in section 16.1.2 could now be repeated for this new choice of basis and reference points, leading to a new set of applied loads, $\underline{\mathcal{A}}_\ell'^+$, deformation measures, $\underline{\mathcal{E}}_\ell'^+$, tangent operator, $\underline{\underline{\mathcal{H}}}(\underline{\mathcal{E}}_\ell'^+)$, and associated generalized forces, $\underline{\mathcal{L}}_\ell'^+$.

If the same problem is treated with scenario ℓ in the two different frames, the sets of loads applied at points $\mathbf{L}$ and $\mathbf{L}'$ must be *equipollent*, which implies

$$\underline{\mathcal{A}}_\ell^+ = \underline{\underline{\mathcal{C}}}'^{-T}(\underline{s}, \underline{\underline{S}})\underline{\mathcal{A}}_\ell'^+. \tag{16.14}$$

This equation expresses the relationship between the components of the loading vector in the two frames, $\mathcal{F}_0$ to $\mathcal{F}_0'$, *i.e.*, the equipollence condition implies that the loading vector is a first-order tensor, see eq. (16.5).

To be physically meaningful, the corresponding deformation measures must also be invariant with respect to a change of frame, *i.e.*, they must also be first-order tensors, and their components in two frames, $\mathcal{F}_0$ and $\mathcal{F}_0'$, denoted $\underline{\mathcal{E}}_\ell^+$ and $\underline{\mathcal{E}}_\ell'^+$, respectively, must transform according to the rules of transformation for kinematic quantities given by eq. (16.4), *i.e.*,

$$\underline{\mathcal{E}}_\ell^+ = \underline{\underline{\mathcal{C}}}'(\underline{s}, \underline{\underline{S}})\underline{\mathcal{E}}_\ell'^+. \tag{16.15}$$

This equation expresses the desired invariance of the deformation measure.

The motion tensor is a second-order tensor and the deformation measure is a parameterization of this motion tensor. According to eq. (16.15), this parameterization must be a first-order tensor. This implies that the deformation measure must be a tensorial parameterization of motion.

16.1.5 Deformation measure invariance

Equation (16.6) expresses the invariance of the differential work with respect to a change of frame. The equipollence condition of the applied load is expressed by eq. (16.14) and introducing this condition into eq. (16.6) yields

$$\underline{\mathrm{d}\mathcal{U}}_\ell^+ = \underline{\underline{\mathcal{C}}}'(\underline{s}, \underline{\underline{S}})\underline{\mathrm{d}\mathcal{U}}_\ell'^+. \tag{16.16}$$

The equipollence of the applied load and invariance of the differential work imply that the components of the loading vector transform according to the first-order tensor transformation rule expressed by eq. (16.5) for loading quantities and the components of the differential displacement vector according to that expressed by eq. (16.4) for kinematic quantities.

Introducing eq. (16.16) into eq. (16.7) and pre-multiplying by $\underline{\underline{\mathcal{C}}}'^{-1}$ yields $\underline{\mathrm{d}\mathcal{U}}_\ell'^+ = \underline{\underline{\mathcal{C}}}'^{-1}\underline{\underline{\mathcal{H}}}(\underline{\mathcal{E}}_\ell^+)\underline{\underline{\mathcal{C}}}'\underline{\underline{\mathcal{C}}}'^{-1}\mathrm{d}\underline{\mathcal{E}}_\ell^+$, where $\underline{\underline{\mathcal{C}}}'\underline{\underline{\mathcal{C}}}'^{-1} = \underline{\underline{\mathcal{I}}}$. Introducing eq. (14.59) then yields $\underline{\mathrm{d}\mathcal{U}}_\ell'^+ = \underline{\underline{\mathcal{H}}}(\underline{\mathcal{E}}_\ell'^+)\underline{\underline{\mathcal{C}}}'^{-1}\mathrm{d}\underline{\mathcal{E}}_\ell^+$, which leads to the expected transformation rule for the components of the differential deformation measure

$$\mathrm{d}\underline{\mathcal{E}}_\ell^+ = \underline{\underline{\mathcal{C}}}'\mathrm{d}\underline{\mathcal{E}}_\ell'^+. \tag{16.17}$$

The invariance of the differential work written in the form of eq. (16.8) requires $\mathrm{d}W = \underline{\mathcal{L}}_\ell^{+T}\mathrm{d}\underline{\mathcal{E}}_\ell^+ = \underline{\mathcal{L}}_\ell'^{+T}\mathrm{d}\underline{\mathcal{E}}_\ell'^+$. Introducing eq. (16.17) then yields

$$\underline{\mathcal{L}}_\ell^+ = \underline{\underline{C}}'^{-T}\,\underline{\mathcal{L}}_\ell'^+. \tag{16.18}$$

In summary, the formulation developed in section 16.1.2, is frame invariant. Under a change of frame, the components of the applied and generalized loads transform according to eqs. (16.14) and (16.18), respectively. The components of the deformation measure, differential displacement, and differential deformation measure transform according to eqs. (16.15), (16.16), and (16.17), respectively. These energetically conjugate first-order tensors present different transformation rules under a change of frame to guarantee the required invariance of the differential work.

The invariance of the various quantities involved in the formulation stems from the tensorial nature of the deformation measure. Because this measure is selected to be the tensorial parameterization of motion, it must be an eigenvector of the motion tensor, *i.e.*, $\underline{\mathcal{E}}_\ell^+ = \underline{\underline{C}}\,\underline{\mathcal{E}}_\ell^+$. Since the deformation measure is a kinematic quantity, $\underline{\mathcal{E}}_\ell^+ = \underline{\underline{C}}\,\underline{\mathcal{E}}_\ell^*$, and it follows that $\underline{\mathcal{E}}_\ell^+ = \underline{\mathcal{E}}_\ell^*$, *i.e.*, the components of the deformation measure are identical in frames $\mathcal{F}_0$ and $\mathcal{F}^\ell$. This implies that the deformation measure is identical when viewed by observers in frames $\mathcal{F}_0$ or $\mathcal{F}^\ell$. Consequently, the deformation measure is not biased towards one of the nodes of the joint, a shortcoming of many of the formulation presently implemented in research and commercial codes.

Equation (16.12) implies $\underline{\mathcal{E}}_k^+ = -\underline{\mathcal{E}}_\ell^+$, which simply corresponds to a sign convention. Henceforth, notation $\underline{\mathcal{E}} = \underline{\mathcal{E}}_\ell^+ = \underline{\mathcal{E}}_\ell^*$ is used, which emphasizes the intrinsic nature of the deformation measure; of course, a change of sign is required for scenario k. Finally, eq. (16.10) implies $\underline{\mathcal{L}} = \underline{\mathcal{L}}_\ell^+ = \underline{\mathcal{L}}_\ell^*$, which shows the intrinsic nature of the generalized forces; here again, a change of sign is required for scenario k.

The proposed deformation measures are parallel to the eigenvector of the motion tensor associated with its unit eigenvalue. Because this eigenvalue has a multiplicity of two, two linearly independent eigenvectors exist, and the deformation measure is a linear combination of these two eigenvectors. An explicit expression of the deformation measure, see eq. (14.37), is

$$\underline{\mathcal{E}} = \begin{Bmatrix} \underline{\epsilon} \\ \underline{\kappa} \end{Bmatrix} = \begin{Bmatrix} \underline{\underline{D}}(\underline{\kappa})\underline{u} \\ \underline{\kappa} \end{Bmatrix}, \tag{16.19}$$

where the stretch vector, $\underline{\epsilon}$, is related to the displacement vector, $\underline{u}$, of the handle, the wryness vector, $\underline{\kappa}$, is the vectorial parameterization of rotation, and tensor $\underline{\underline{D}}$ is defined by eq. (14.38).

16.1.6 Flexible joint constitutive laws

The strain energy of the flexible joint is assumed to be a quadratic function of the deformation measures, $A = 1/2\ \underline{\mathcal{E}}^T\,\underline{\underline{K}}\,\underline{\mathcal{E}}$, where $\underline{\underline{K}}$ is the joint's stiffness matrix for infinitesimal deformations. The generalized forces now become $\underline{\mathcal{L}} = \underline{\underline{K}}\,\underline{\mathcal{E}}$, and eq. (16.9) then yields

$$\underline{\mathcal{A}}_\ell^+ = \underline{\underline{\mathcal{H}}}^{-T}(\underline{\mathcal{E}})\,\underline{\underline{K}}\,\underline{\mathcal{E}}, \tag{16.20a}$$

$$\underline{\mathcal{A}}_\ell^* = \underline{\underline{\mathcal{H}}}^{*-T}(\underline{\mathcal{E}})\,\underline{\underline{K}}\,\underline{\mathcal{E}}. \tag{16.20b}$$

Due to the presence of the tangent tensor, the load-deformation relationships are nonlinear, and the deformation-displacement relationships, eqs. (16.19), are also nonlinear.

The loads applied to handle ℓ resolved in basis $\mathcal{B}_0$, denoted $\underline{\mathcal{A}}$, are $\underline{\mathcal{A}} = \underline{\underline{\mathcal{T}}}^T \underline{\mathcal{A}}_\ell^+ = \underline{\underline{\mathcal{R}}}\, \underline{\mathcal{A}}_\ell^*$. The joint's constitutive laws now become

$$\underline{\mathcal{A}} = \begin{bmatrix} \underline{\underline{F}}^{-T}(\underline{\kappa}) & \underline{\underline{0}} \\ -\underline{\underline{H}}^{-T}(\underline{\kappa})\underline{\underline{L}}^T(\underline{\epsilon},\underline{\kappa})\underline{\underline{F}}^{-T}(\underline{\kappa}) & \underline{\underline{H}}^{-T}(\underline{\kappa}) \end{bmatrix} \underline{\underline{K}}\, \underline{\mathcal{E}}. \tag{16.21}$$

where tensors $\underline{\underline{F}}$, $\underline{\underline{H}}$, and $\underline{\underline{L}}$ are defined by eqs. (14.41), (13.55), and (14.46), respectively.

Finally, inversion of this equation gives the constitutive laws in compliance form as

$$\underline{\mathcal{E}} = \underline{\underline{S}} \begin{bmatrix} \underline{\underline{F}}^T(\underline{\kappa}) & \underline{\underline{0}} \\ \underline{\underline{L}}^T(\underline{\epsilon},\underline{\kappa}) & \underline{\underline{H}}^T(\underline{\kappa}) \end{bmatrix} \underline{\mathcal{A}}, \tag{16.22}$$

where $\underline{\underline{S}} = \underline{\underline{K}}^{-1}$ is the compliance matrix for infinitesimal deformations. Given the externally applied loads, $\underline{\mathcal{A}}$, this nonlinear equation yield the joints deformations, in terms of the stretch vector, $\underline{\epsilon}$, and the wryness vector, $\underline{\kappa}$.

This section has focused on the definition of appropriate deformation measures for elastic bodies of finite dimension, in contrast with classical strain measures that are defined for infinitesimal elements of an elastic body. It was first argued that to be physically meaningful, these deformation measures must be of a tensorial nature. Next, it was proved that this requirement is satisfied if and only if the deformation measures are parallel to the eigenvector of the motion tensor associated with its unit eigenvalue.

Equipped with these deformation measures, constitutive laws for the flexible joint were derived by assuming the existence of a strain energy function that is a quadratic form of these deformation measures. Because all the quantities involved in the formulation are of a tensorial nature, the behavior of the joint presents the required invariance with respect to changes of basis or reference point. Furthermore, the proposed strain measures are unbiased. Flexible joint formulations described in the literature up to date do not appear to present these desirable characteristics.

Example 16.1. Simple beam treated as a flexible joint

The load-deformation and deformation-configuration relationships developed above will be tested on a number of simple examples involving a flexible beam. Figure 16.4 shows the beam of length L along unit vector $\bar{b}_{01}$, width b along $\bar{b}_{02}$, and height h along $\bar{b}_{03}$. The beam is made of a homogeneous material of Young's modulus E and shear modulus G. The examples presented below use the following data: $L = 0.6$ m, $b = 5$ mm, $h = 15$ mm, $E = 73$ GPa, and $G = E/(2(1+\nu))$, where $\nu = 0.3$.

Handles k and ℓ are rigidly attached to the root and tip of the beam, respectively. Elementary structural analysis [285] yields the compliance matrix of the joint

$$\underline{\underline{S}} = \begin{bmatrix} L/S & 0 & 0 & 0 & 0 & 0 \\ 0 & L^3/3H_{33} & 0 & 0 & 0 & L^2/2H_{33} \\ 0 & 0 & L^3/3H_{22} & 0 & -L^2/2H_{22} & 0 \\ 0 & 0 & 0 & L/H_{11} & 0 & 0 \\ 0 & 0 & -L^2/2H_{22} & 0 & L/H_{22} & 0 \\ 0 & L^2/2H_{33} & 0 & 0 & 0 & L/H_{33} \end{bmatrix}, \tag{16.23}$$

where $S = Ebh$, $H_{22} = Ebh^3/12$, $H_{33} = Ehb^3/12$, and $H_{11} = Ghb^3/3$ are the beam's axial stiffness, bending stiffness with respect the unit vector $\bar{\imath}_2$, bending stiffness with respect the unit vector $\bar{\imath}_3$, and torsional stiffness, respectively.

Various combinations of forces and moments are applied to handle k, and the resulting displacements and rotations are then evaluated using the joint's constitutive laws, eqs. (16.22). These predictions are compared with those of a finite element solution for the geometrically exact beam model presented in section 16.3, which provide an exact treatment of the kinematics of the system, but assume the strains to remain small at all time. This latter assumption is equivalent to assuming a constant compliance matrix, as done here. All the numerical solutions shown below are obtained by modeling the beam with 12 cubic elements, corresponding to a total 216 degrees of freedom.

In the first example, the joint is subjected to a single bending moment about unit vector $\bar{\imath}_3$, denoted M_3. For this simple case, eqs. (16.22) can be solved analytically to yield $\kappa_3(\phi) = \sigma_0(\phi)\bar{M}_3$, where ϕ is the rotation angle of handle ℓ about unit vector $\bar{\imath}_3$ and $\bar{M}_3 = LM_3/H_{33}$. The displacement components of handle ℓ along unit vectors $\bar{\imath}_1$ and $\bar{\imath}_2$ are then $\bar{u}_1 = u_1/L = -(1-\cos\phi)/2$ and $\bar{u}_2 = u_2/L = 1/2\ \sin\phi$.

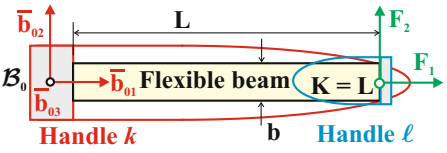

Fig. 16.4. Reference configuration of the flexible beam.

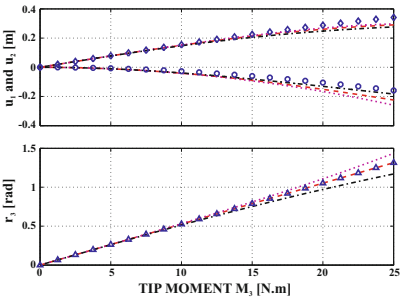

Fig. 16.5. Joint deformation under a single moment. Top figure: displacement components u_1 (○) and u_2 (◇); bottom figure: rotation r_3 (△). Exact solution: symbols. Present solution: $\kappa(\phi) = \phi$, dashed line; $\kappa(\phi) = 4\sin\phi/4$, dotted line; $\kappa(\phi) = 4\tan\phi/4$, dashed-dotted line.

The exact solution of this problem is easily found because the beam deforms into an arc of circle under the single applied moment, leading to $\phi = \bar{M}_3$, $\bar{u}_1 = -(1 - \sin\phi/\phi)/2$, and $\bar{u}_2 = (1 - \cos\phi)/\phi$, see fig. 16.5. Three approximate solutions obtained from the proposed approach for three different generating functions, $\kappa(\phi) = \phi$, $\kappa(\phi) = 4\sin\phi/4$, and $\kappa(\phi) = 4\tan\phi/4$, are also depicted in this figure. For $\kappa(\phi) = \phi$, corresponding to the exponential map of rotation, the proposed approach gives the exact solution of the joint's relative rotation. The transverse displacement of the joint is well captured up to very large displacement magnitudes, $u_2 \approx 0.3$ m, for a beam of length $L = 0.6$ m. The beam's foreshortening, a higher-order nonlinear effect, is also well predicted up to large transverse displacements.

If the joint were made of a nonlinear material, the curvature-relative rotation relationship would become nonlinear, and the generating function could be selected to approximate this numerically or experimentally observed behavior as closely as possible. This will enable the present approach to deal with nonlinear elastic manner in an approximate manner. This effect is apparent in fig 16.5 that depicts the curvature-relative rotation relationship for generating functions $\kappa(\phi) = 4\sin\phi/4$ and $\kappa(\phi) = 4\tan\phi/4$, which give rise to softening or stiffening material behaviors, respectively.

The second example involves the same flexible joint now subjected to two moment components, $M_2 = 3\lambda$ N·m and $M_3 = \lambda$ N·m, acting about unit vectors $\bar{\imath}_2$ and $\bar{\imath}_3$, respectively, where $\lambda \in [0, 12]$ is the loading factor.

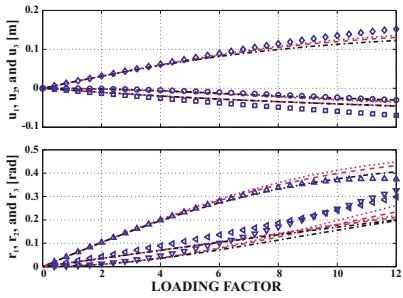

Fig. 16.6. Joint deformation under two moments. Top figure: displacement components u_1 (○), u_2 (◇), and u_3 (□); bottom figure: exponential map components r_1 (▽), r_2 (◁), and r_3 (△). Finite element solution: symbols. Present solution: $\kappa(\phi) = \phi$, dashed line; $\kappa(\phi) = 2\sin\phi/2$, dotted line; $\kappa(\phi) = 2\tan\phi/2$, dashed-dotted line.

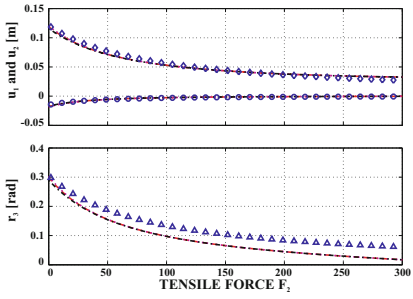

Fig. 16.7. Joint deformation under two forces. Top figure: displacement components u_1 (○) and u_2 (◇); bottom figure: exponential map component r_3 (△). Finite element solution: symbols. Present solution: $\kappa(\phi) = \phi$, dashed line; $\kappa(\phi) = 2\sin\phi/2$, dotted line; $\kappa(\phi) = 2\tan\phi/2$, dashed-dotted line.

Figure 16.6 illustrate the ability of the proposed approach to capture the coupled, three-dimensional response of the joint up to large relative displacements and rotations.

In the next example, the joint is subjected to two forces: a constant force $F_2 = 20$ N and a linearly increasing tensile force $F_1 \in [0, 300]$ N, acting along unit vectors $\bar{\imath}_2$ and $\bar{\imath}_1$, respectively. Under the effect of the tensile force, the joint stiffens and the displacement component u_2 resulting from the constant force component F_2 decreases, as shown in fig. 16.7. Here again, the predictions of the proposed approach are found to be in qualitative agreement with the finite element solution.

The stiffening of the joint under a tensile force is a nonlinear effect that is captured by the proposed approach because the equilibrium equations of the joint are expressed in the deformed configuration of the system. This prompts the following question: is the proposed formulation able to predict the instability of the joint under compressive load?

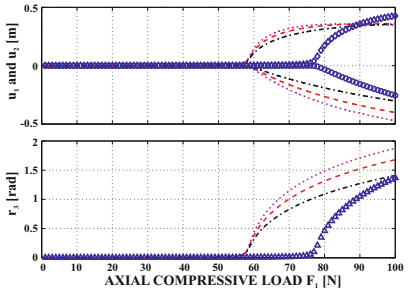

Fig. 16.8. Joint deformation under compressive force. Top figure: displacement components u_1 ($\circ$) and u_2 ($\diamond$); bottom figure: exponential map component r_3 ($\triangle$). Finite element solution: symbols. Present solution: $\kappa(\phi) = \phi$, dashed line; $\kappa(\phi) = 4\sin\phi/4$, dotted line; $\kappa(\phi) = 4\tan\phi/4$, dashed-dotted line.

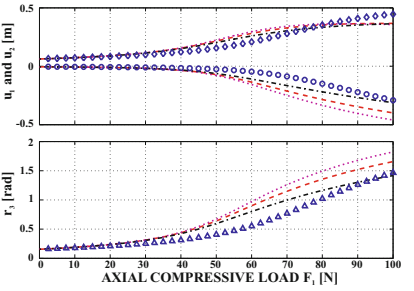

Fig. 16.9. Joint deformation under two forces. Top figure: displacement components u_1 ($\circ$) and u_2 ($\diamond$); bottom figure: exponential map component r_3 ($\triangle$). Finite element solution: symbols. Present solution: $\kappa(\phi) = \phi$, dashed line; $\kappa(\phi) = 2\sin\phi/2$, dotted line; $\kappa(\phi) = 2\tan\phi/2$, dashed-dotted line.

Figure 16.8 shows the response of the system subjected to a small, constant load $F_2 = 0.1$ N and a linearly increasing compressive load, $F_1 \in [0, 100]$ N. The Euler buckling load of the beam [285] is $P_{\text{Euler}} = \pi^2 H_{33}/(4L^2) = 78$ N, which is accurately predicted by the finite element model. The present model also predicts the buckling phenomenon, although for a lower compressive load of about 60 N. The inaccurate prediction of the present model is due to the fact that it uses 6 degrees of freedom only, in contrast with the 216 degrees of freedom used in the reference solution. Modeling the problem with a single two-node beam element also results in an inaccurate prediction of the buckling load, which is over-predicted by about 50%.

It is also possible to trace the post-buckling path of the system. If a constant load $F_2 = 10$ N and a compressive load $F_1 \in [0, 100]$ N are applied to the joint, it quickly enters the post-buckling regime, as depicted in fig. 16.9. The proposed model

traces the post-buckling path for up to very large displacements and rotations: for a compressive load of 100 N, the relative rotation of the joint is of about 180 degrees.

All the predictions presented in this example are in good qualitative agreement with exact solutions for geometrically exact beams obtained from nonlinear finite element simulations, up to very large relative displacements and rotations of the flexible joint. For small to moderate displacements and rotations, the agreement between the predictions of the proposed formulation and exact solutions is accurate.

It must be emphasized that the present formulation only "knows" the linearized compliance matrix of the joint. The nonlinear governing equations of geometrically exact beams are not derived. Yet, the proposed deformation measures used in conjunction with the linearized compliance matrix provide constitutive laws for the flexible joint that qualitatively describe its behavior up to large relative displacements and rotations. Instabilities, such as buckling under large compressive load or lateral buckling under large transverse loads (not shown here for brevity sake) are also predicted by the proposed formulation. For small displacements and rotations, accurate predictions are obtained.

While the proposed deformation measures remain tensorial for deformations of arbitrary magnitude, nonlinear constitutive laws should be used if the joint undergoes large deformations. The numerical examples presented in this example use linear constitutive laws to model a joint consisting of a simple flexible beam. The behavior joint is accurately predicted for small and moderate deformations and the correct qualitative behavior for up to very large displacements and rotations is observed.

16.2 Formulation of cable equations

Cables are one-dimensional, flexible structures that can only carry axial forces, *i.e.*, forces acting in the direction tangent to the cable. In contrast with beams, described in section 16.3, cables present no bending, torsional, or shearing stiffness. The kinematic description of cable structures in presented in section 16.2.1 and leads to the definition of the strain components in section 16.2.2. The governing equations for the static behavior of elastic cables are derived in section 16.2.3 and section 16.2.4 extends the formulation to dynamics problems.

16.2.1 The kinematics of the problem

Figure 16.10 shows a flexible cable idealized as a curve in space. The reference and deformed configurations of the cable will be described with respect to an inertial reference frame, $\mathcal{F}^I = [\mathbf{O}, \mathcal{I} = (\bar{\imath}_1, \bar{\imath}_2, \bar{\imath}_3)]$. Material point $\mathbf{P}$ of the cable is defined by its curvilinear coordinate, α_1, which measures length along the reference configuration of the cable.

The position vector of point $\mathbf{P}$ is

$$\underline{x} = \underline{x}(\alpha_1). \tag{16.24}$$

Using eq. (15.26), base vector $\bar{g}_1$ becomes

$$\bar{g}_1 = \frac{\partial \underline{x}}{\partial \alpha_1}. \tag{16.25}$$

The base vector is the unit tangent to the curve that defines the geometry of the cable in its reference configuration; indeed, as discussed in section 2.2.1, curvilinear variable α_1 represents an intrinsic parameterization of the curve.

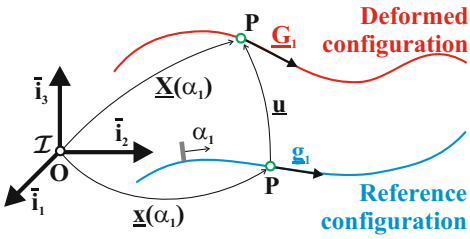

Fig. 16.10. Cable in the reference and deformed configurations.

In the deformed configuration, the position vector of point **P**, denoted $\underline{X}(\alpha_1)$, becomes

$$\underline{X}(\alpha_1) = \underline{x}(\alpha_1) + \underline{u}(\alpha_1), \tag{16.26}$$

where $\underline{u}$ is the displacement vector of point **P**. The base vector in the deformed configuration becomes

$$\underline{G}_1 = \frac{\partial \underline{X}}{\partial \alpha_1} = \bar{g}_1 + \underline{u}' \tag{16.27}$$

where notation $(\cdot)'$ indicates a derivative with respect to α_1. Because the cable undergoes axial deformations, material coordinate α_1 no longer measures length along the deformed configuration of the cable; hence, as discussed in section 2.2.2, it represents an arbitrary parameterization of the curve defining the geometry of the cable in its deformed configuration. Base vector $\underline{G}_1$ is tangent to the deformed configuration of the cable, but it is not a unit vector.

Let unit vector $\bar{\jmath}_1$ be parallel to base vector $\underline{G}_1$,

$$\underline{G}_1 = (1 + \bar{e}_{11})\, \bar{\jmath}_1, \tag{16.28}$$

where $\bar{e}_{11}$ is a strain related parameter which can be expressed in terms of displacements with the help of eqs. (16.27) and (16.28)

$$(1 + \bar{e}_{11})^2 = (\bar{g}_1 + \underline{u}')^T (\bar{g}_1 + \underline{u}'). \tag{16.29}$$

Because the cable is a one dimensional structure, the metric tensor reduces to a single component, $G_{11} = (1 + \bar{e}_{11})^2$. The only non vanishing component of the Green-Lagrange strain tensor, eq. (15.45), is

$$e_{11} = \frac{1}{2}\left[(1 + \bar{e}_{11})^2 - 1\right] = \bar{e}_{11} + \frac{1}{2}\bar{e}_{11}^2 = \bar{g}_1^T \underline{u}' + \frac{1}{2}\underline{u}'^T \underline{u}', \tag{16.30}$$

where the strain parameter was expressed in terms of displacement using eq. (16.29).

16.2.2 The small strain assumption

The strain-displacement relation, eq. (16.30), is valid for arbitrarily large displacements and strains. If the strain component can be assumed to remain much smaller

that unity, a simplified strain-displacement relationship can be obtained. The modified deformation gradient tensor defined in section 15.5.1 reduces to a single component, $\hat{F}_{11}$, obtained from eqs. (15.65) and (16.28) as

$$\hat{F}_{11} = 1 + \bar{e}_{11}. \tag{16.31}$$

The small strain measure then follows from eq. (15.73)

$$\gamma_{11} = \bar{e}_{11} \approx \bar{g}_1^T \underline{u}' + \frac{1}{2} \underline{u}'^T \underline{u}'. \tag{16.32}$$

The small strain assumption was used to approximate eq. (16.30), $e_{11} = \bar{e}_{11} + \bar{e}_{11}^2/2 \approx \bar{e}_{11}$, leading to the second equality of eq. (16.32). When the strains are small, it is clear that the strain parameter, $\bar{e}_{11}$, is equal to the axial strain in the cable, γ_{11}. Variation of the small strain measure is

$$\delta\gamma_{11} = \delta\underline{u}'^T (\bar{g}_1 + \underline{u}') = \delta\underline{u}'^T \underline{G}_1. \tag{16.33}$$

16.2.3 Governing equations

The governing equations of the static problem are readily obtained from the principle of virtual work, eq. (15.72), which states

$$\int_0^L \int_{\mathcal{A}} \tau^{*11} \delta\gamma_{11} \, \mathrm{d}\mathcal{A} \mathrm{d}\alpha_1 = \delta W_{\text{ext}}, \tag{16.34}$$

for all arbitrary virtual displacements. The length of the cable in the reference configuration is denoted L, $\mathcal{A}$ is its cross-section area, and δW_{ext} the virtual work done by the externally applied loads. Integrating the left-hand side over the cross-sectional area of the cable yields

$$\int_0^L F^* \delta\gamma_{11} \, \mathrm{d}\alpha_1 = \delta W_{\text{ext}}, \tag{16.35}$$

where $F^* = \int_{\mathcal{A}} \tau^{*11} \, \mathrm{d}\mathcal{A}$ is the total axial force in the cable along material axis $\bar{\jmath}_1$.

The virtual work done by the forces externally applied to the cable is expressed as $\delta W_{\text{ext}} = \int_0^L \delta\underline{u}^T \underline{f} \, \mathrm{d}\alpha_1$, where $\underline{f}$ is the externally applied load per unit length of the cable's reference configuration. Introducing the strain variation, eq. (16.33), into eq. (16.35) then leads to

$$\int_0^L \delta\underline{u}'^T F^* \underline{G}_1 \, \mathrm{d}\alpha_1 = \int_0^L \delta\underline{u}^T \underline{f} \, \mathrm{d}\alpha_1. \tag{16.36}$$

Integration by parts then yields the governing equations of the problem,

$$[F^* \underline{G}_1]' = -\underline{f}. \tag{16.37}$$

If the cable is assumed to present a linear elastic behavior, the constitutive law simply states the proportionality of the axial force to the axial strain,

$$F^* = S\gamma_{11}, \tag{16.38}$$

where S is the axial stiffness of the cable. Introducing the constitutive law into the governing equation, eq. (16.37),

$$\left[S\underline{u}'^T(\bar{g}_1 + \underline{u}'/2)\underline{G}_1\right]' = -\underline{f}. \tag{16.39}$$

When written in this form, the high level of nonlinearity of the equation governing the cable's displacement field is apparent.

16.2.4 Extension to dynamic problems

The formulation presented thus far has focused on static problems. If the cable's configuration changes in time, the inertial velocity of a material point of the cable is $\underline{v} = \dot{\underline{u}}$. The cable's total kinetic energy is then

$$K = \frac{1}{2}\int_0^L \int_{\mathcal{A}} \rho \dot{\underline{u}}^T \dot{\underline{u}}\, \mathrm{d}\mathcal{A}\mathrm{d}\alpha_1 = \frac{1}{2}\int_0^L m\dot{\underline{u}}^T \dot{\underline{u}}\, \mathrm{d}\alpha_1, \tag{16.40}$$

where ρ is the cable's mass density, and $m = \int_{\mathcal{A}} \rho\, \mathrm{d}\mathcal{A}$ its mass per unit span in the reference configuration.

Variation of the kinetic energy is

$$\delta K = \int_0^L \delta\dot{\underline{u}}^T m\dot{\underline{u}}\, \mathrm{d}\alpha_1 = \int_0^L \delta\dot{\underline{u}}^T \underline{p}\, \mathrm{d}\alpha_1, \tag{16.41}$$

where $\underline{p} = m\dot{\underline{u}}$ is the momentum vector. Hamilton's principle now yields the equations of motion of the problem

$$m\ddot{\underline{u}} - [F^*\underline{G}_1]' = \underline{f}. \tag{16.42}$$

These equations of motion are valid for arbitrarily large displacements of the cable when the strain components are assumed to remain small.

16.2.5 Problems

Problem 16.1. Linear elastic cable
Consider a cable with a linear elastic constitutive law: $F^* = S\,\gamma_{11}$, where S is the axial stiffness of the cable. The cable is unloaded. Prove: *(1)* the preservation the total linear momentum of the cable; *(2)* the preservation the total angular momentum of the cable; *(3)* the preservation the total mechanical energy of the cable. If the cable is subjected to distributed external loads $\underline{f}(\alpha_1, t)$ and end forces $F_1(t)$ and $F_2(t)$ at $\alpha_1 = 0$ and L, respectively, what happens to the above three preservation laws?

Problem 16.2. Pre-stretched cable
Consider a straight, pre-stretched cable of length L. The constitutive law for the cable is $F^* = S\,(\bar{e}+\gamma_{11})$, where $\bar{e}$ is the pre-stretch, S the axial stiffness, and hence, $T = S\,\bar{e}$ the pre-tension in the cable. Linearize the governing equations by assuming displacement field to remain small. Find the equilibrium configuration of the cable under a uniform transverse loading f_0. For the unloaded cable under pre-tension find the natural frequencies and mode shapes of the system.

16.3 Formulation of beam equations

A beam is defined as a structure having one of its dimensions much larger than the other two. The axis of the beam is defined along that longer dimension and its cross-section is normal to this axis. The cross-section's geometric and physical properties are assumed to vary smoothly along the beam's span. Civil engineering structures often consist of assemblies or grids of beams with cross-sections having shapes such as T's or I's. A large number of machine parts also are beam-like structures: linkages, transmission shafts, robotic arms, etc. Aeronautical structures such as aircraft wings or helicopter rotor blades are often treated as thin-walled beams. Finally, both tower and rotor blades of wind turbines also fall within the category of beams structures.

The solid mechanics theory of beams, more commonly referred to simply as "beam theory," plays an important role in structural analysis because it provides designers with simple tools to analyze numerous structures [285]. Within the framework of multibody dynamics, the governing equations for beam structures are nonlinear partial differential equations, and the finite element method is often used to obtain approximate numerical solutions of these equations. Of course, the same finite element approach could also be used to model the same structures based on plate and shell, or even three-dimensional elasticity models, but at a much higher computation cost. Beam models are often used at a pre-design stage because they provide valuable insight into the behavior of structures.

Several beam theories have been developed based on various assumptions, and lead to different levels of accuracy. One of the simplest and most useful of these theories is due to Euler who analyzed the elastic deformation of a slender beam, a problem known as Euler's Elastica [297]. Euler-Bernoulli beam theory [285] is now commonly used in many civil, mechanical and aerospace applications, although shear deformable beam theories [298, 299], often called "Timoshenko beams," have also found wide acceptance. Reissner investigated beam theory for large strains [300] and large displacements of spatially curved members [301, 302].

In this section, the *geometrically exact beam theory* will be presented. The kinematic description of the problem developed in section 16.3.1 accounts for arbitrarily large displacements and rotation, hence the term "geometrically exact," although the strain components are assumed to remain small, see section 15.5.2. The kinematics of geometrically beams was first presented by Simo *et al.* [303, 304], but similar developments were proposed by Borri and Merlini [305] or Danielson and Hodges [306, 307].

In many applications, however, beams are, in fact, complex build-up structures with solid or thin-walled cross-sections. In aeronautical constructions, for instance, the increasing use of laminated composite materials leads to heterogeneous, highly anisotropic structures. The analysis of complex cross-sections featuring composite materials and the determination of the associated sectional properties was first presented by Giavotto *et al.* [308, 309]. Their approach, based on linear elasticity theory, leads to a two-dimensional analysis of the beam's cross-section using finite elements, which yields the sectional stiffness characteristics in the form of a 6×6 stiffness matrix relating the six sectional deformations, three strains and three curvatures, to the

sectional loads, three forces and three moments. Furthermore, the three-dimensional strain field at all points of the cross-section can be recovered once the sectional strains are known.

For nonlinear problems, the decomposition of the beam problem into a linear, two-dimensional analysis over the cross-section, and a nonlinear, one-dimensional analysis along its span was first proposed by Berdichevsky [310]. Hodges [311] has reviewed many approaches to beam modeling; he points out that although the two-dimensional finite element analysis of the cross-section seems to be computationally expensive, it is, in fact, a preprocessing step that is performed once only.

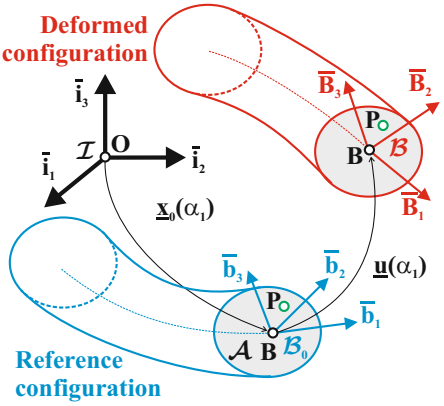

Fig. 16.11. Curved beam in the reference and deformed configurations.

A unified theory presenting both linear, two-dimensional analysis over the cross-section, and a nonlinear, one-dimensional analysis along the beam's span was further refined by Hodges and his co-workers [312, 313]. The nonlinear, one-dimensional analysis along the beam's span corresponds the geometrically exact beam theory developed earlier based on simplified kinematic assumptions. More sophisticated beam theories have been developed that account for Vlasov effects [314] or the trapeze effect [315]. Detailed developments of nonlinear composite beam theory developed by Hodges and his coworkers are found in his textbook [316] and applications to multibody systems in ref. [283].

16.3.1 Kinematics of the problem

Figure 16.11 depicts an initially curved and twisted beam of length L, with a cross-section of arbitrary shape and area $\mathcal{A}$. The volume of the beam is generated by sliding the cross-section along the reference line of the beam, which is defined by an arbitrary curve in space. Curvilinear coordinate α_1 defines the intrinsic parameterization of this curve, section 2.2.1, *i.e.*, it measures length along the beam's reference line. Point **B** is located at the intersection of the reference line with the plane of the cross-section.

In the reference configuration, an orthonormal basis, $\mathcal{B}_0(\alpha_1) = (\bar{b}_1, \bar{b}_2, \bar{b}_3)$, is defined at point **B**. Vector $\bar{b}_1$ is the unit tangent vector to the reference curve at that point, and unit vectors $\bar{b}_2$ and $\bar{b}_3$ define the plane to the cross-section. An inertial reference frame, $\mathcal{F}^I = [\mathbf{O}, \mathcal{I} = (\bar{\imath}_1, \bar{\imath}_2, \bar{\imath}_3)]$, is defined, and the components of the rotation tensor that brings basis $\mathcal{I}$ to $\mathcal{B}_0$, resolved in basis $\mathcal{I}$, are denoted $\underline{\underline{R}}_0(\alpha_1)$.

The position vector of point **B** along the beam's reference line is denoted $\underline{x}_0(\alpha_1)$. The position vector of material point **P** of the beam then becomes $\underline{x}(\alpha_1, \alpha_2, \alpha_3) = \underline{x}_0(\alpha_1) + \alpha_2\, \bar{b}_2 + \alpha_3\, \bar{b}_3$, where α_2 and α_3 are the material

coordinates along unit vectors $\bar{b}_2$ and $\bar{b}_3$, respectively. Coordinates α_1, α_2, and α_3 form a natural choice of coordinates to represent the configuration of the beam.

The displacement field

In the deformed configuration, all the material points located on a cross-section of the beam move to new positions. This motion is decomposed into two parts, a rigid body motion and a warping displacement field. The rigid body motion consists of a translation of the cross-section, characterized by displacement vector $\underline{u}(\alpha_1)$ of reference point **B**, and of a rotation of the cross-section, which brings basis $\mathcal{B}_0$ to $\mathcal{B}(\alpha_1) = (\bar{B}_1, \bar{B}_2, \bar{B}_3)$, see fig. 16.11. The components of the rotation tensor that brings basis $\mathcal{B}_0$ to $\mathcal{B}$, resolved in basis $\mathcal{I}$, are denoted $\underline{\underline{R}}(\alpha_1)$.

The warping displacement field is defined as $\underline{w}(\alpha_1, \alpha_2, \alpha_3) = w_1\bar{B}_1 + w_2\bar{B}_2 + w_3\bar{B}_3$. This displacement field represents a warping that includes both in-plane and out-of-plane deformations of the cross-section. To be uniquely defined, the warping field should be orthogonal to the rigid body motion [308, 316]. Consequently, unit vectors $\bar{B}_2$ and $\bar{B}_3$ define the average plane of the cross-section and vector $\bar{B}_1$ is orthogonal to that plane.

The position vector of point **P** in the deformed configuration now becomes

$$\underline{X}(\alpha_1, \alpha_2, \alpha_3) = \underline{X}_0 + w_1\ \bar{B}_1 + (w_2 + \alpha_2)\bar{B}_2 + (w_3 + \alpha_3)\bar{B}_3. \tag{16.43}$$

The position of point **B** is expressed as $\underline{X}_0(\alpha_1) = \underline{x}_0 + \underline{u}$. Because $\bar{B}_i = \underline{\underline{R}}\ \bar{b}_i = (\underline{\underline{R}}\,\underline{\underline{R}}_0)\ \bar{\imath}_i$, eq. (16.43) becomes

$$\underline{X}(\alpha_1, \alpha_2, \alpha_3) = \underline{x}_0 + \underline{u} + (\underline{\underline{R}}\,\underline{\underline{R}}_0)\,(\underline{w} + \alpha_2\ \bar{\imath}_2 + \alpha_3\ \bar{\imath}_3)\,. \tag{16.44}$$

The warping displacement field is computed from the geometric and stiffness properties of the cross-section, typically by solving a two-dimensional finite element problem over the cross-section, as described in refs. [308, 316].

The sectional strain measures

The sectional strain measures for beams with shallow curvature are defined as

$$\underline{e} = \begin{Bmatrix} \underline{\epsilon} \\ \underline{\kappa} \end{Bmatrix} = \begin{Bmatrix} \underline{x}_0' + \underline{u}' - (\underline{\underline{R}}\,\underline{\underline{R}}_0)\ \bar{\imath}_1, \\ \underline{k} + \underline{\underline{R}}\,\underline{k}_i \end{Bmatrix}, \tag{16.45}$$

where $\underline{k} = \text{axial}(\underline{\underline{R}}'\underline{\underline{R}}^T)$ are the components of the sectional curvature vector resolved in the inertial basis and $\underline{k}_i$ the components of the corresponding curvature vector in the reference configuration. Notation $(\cdot)'$ indicates a derivative with respect to α_1. The strain components resolved in the convected material basis, $\mathcal{B}$, are denoted $\underline{\epsilon}^* = (\underline{\underline{R}}\,\underline{\underline{R}}_0)^T\,\underline{\epsilon}$ and consist of the sectional axial and shear strains. The curvature components resolved in the same material basis are denoted $\underline{\kappa}^* = (\underline{\underline{R}}\,\underline{\underline{R}}_0)^T\,\underline{\kappa}$

and consist of the sectional twisting and bending curvatures. Notation $(\cdot)^*$ indicates the components of vectors and tensors resolved in the material basis.

By definition, a rigid body motion is a motion that generates no strains. This implies that the following rigid body motion, $\underline{u}(\alpha_1) = \underline{u}^R + (\underline{\underline{R}}^R - \underline{\underline{I}})\underline{x}_0(\alpha_1)$, $\underline{\underline{R}}(\alpha_1) = \underline{\underline{R}}^R$, consisting of a translation, $\underline{u}^R$, and a rotation about the origin characterized by a rotation matrix, $\underline{\underline{R}}^R$, should generate no straining of the beam. It can be readily verified with the help of eqs. (16.45) that such rigid body motion results in $\underline{\epsilon} = 0$ and $\underline{\kappa} = 0$, as expected.

16.3.2 Governing equations

For the problem at hand, the principle of virtual work states

$$\int_0^L (\delta\underline{\epsilon}^{*T}\underline{N}^* + \delta\underline{\kappa}^{*T}\underline{M}^*)\,\mathrm{d}\alpha_1 = \delta W_{\mathrm{ext}}, \tag{16.46}$$

where $\underline{N}^*$ and $\underline{M}^*$ are the beam's sectional forces and moments, respectively. The sectional constitutive law relates the sectional strain measures to the sectional loads,

$$\begin{Bmatrix} \underline{N}^* \\ \underline{M}^* \end{Bmatrix} = \underline{\underline{\mathcal{C}}}^* \begin{Bmatrix} \underline{\epsilon}^* \\ \underline{\kappa}^* \end{Bmatrix}, \tag{16.47}$$

where $\underline{\underline{\mathcal{C}}}^*$ is the beam's 6×6 sectional stiffness matrix. This matrix is a byproduct of a two-dimensional finite element analysis over the beam's cross-section, as discussed in refs. [308, 316]. For homogeneous sections of simple geometry, exact or approximate analytical expressions are available for the stiffness matrix.

Variations in strain components are expressed using eq. (16.45) to find

$$\delta\underline{\epsilon}^* = (\underline{\underline{R}}\,\underline{\underline{R}}_0)^T \left[\delta\underline{u}' + (\widetilde{x}_0' + \widetilde{u}')\underline{\delta\psi}\right], \tag{16.48a}$$

$$\delta\underline{\kappa}^* = (\underline{\underline{R}}\,\underline{\underline{R}}_0)^T \underline{\delta\psi}'. \tag{16.48b}$$

where $\underline{\delta\psi} = \mathrm{axial}(\delta\underline{\underline{R}}\,\underline{\underline{R}}^T)$ is the virtual rotation vector. The principle of virtual work, eq. (16.46), now becomes

$$\int_0^L \left\{ \left[\delta\underline{u}'^T + \underline{\delta\psi}^T(\widetilde{x}_0' + \widetilde{u}')^T\right]\underline{N} + \underline{\delta\psi}'^T\underline{M} \right\} \mathrm{d}\alpha_1 = \delta W_{\mathrm{ext}}, \tag{16.49}$$

where $\underline{N} = (\underline{\underline{R}}\,\underline{\underline{R}}_0)\underline{N}^*$ and $\underline{M} = (\underline{\underline{R}}\,\underline{\underline{R}}_0)\underline{M}^*$ are the beam's internal forces and moments, respectively, resolved in the inertial basis.

The virtual work done by the externally applied forces is expressed as $\delta W_{\mathrm{ext}} = \int_0^L [\delta\underline{u}^T\underline{f} + \underline{\delta\psi}^T\underline{m}]\,\mathrm{d}\alpha_1$, where $\underline{f}$ and $\underline{m}$ denote the externally applied forces and moments per unit span of the beam, respectively.

The governing equations of the static problem then follow as

$$\underline{N}' = -\underline{f}, \tag{16.50a}$$

$$\underline{M}' + (\widetilde{x}_0' + \widetilde{u}')\underline{N} = -\underline{m}. \tag{16.50b}$$

Example 16.2. The cantilevered beam under tip loading

Consider a cantilevered beam of length L with a rectangular cross-section of width b and height h. The beam is made of a homogeneous material of Young's modulus E and shear modulus G and is subjected to a tip axial load, N_T, tip transverse load, P_T, and tip moment, M_T. The beam is of bending stiffness $H_{33} = Ebh^3/12$, axial stiffness $S = Ebh$, and shearing stiffness $K_{22} = 5Gbh/6$.

The loading is acting in plane $(\bar{\imath}_1, \bar{\imath}_2)$, and due to the symmetry of the problem, the beam deforms in that plane only. The rotation tensor, $\underline{\underline{R}}$, then corresponds to a planar rotation, eq. (4.6), and the displacement vector, $\underline{u}$, is two-dimensional

$$\underline{\underline{R}} = \begin{bmatrix} C_\theta & -S_\theta \\ S_\theta & C_\theta \end{bmatrix}, \quad \underline{u} = \begin{Bmatrix} u_1 \\ u_2 \end{Bmatrix},$$

where $C_\theta = \cos\theta$, $S_\theta = \sin\theta$, angle θ is the average rotation of the cross-section, and u_1 and u_2 the displacement components along unit vectors $\bar{\imath}_1$ and $\bar{\imath}_2$, respectively.

Because the beam is not subjected to distributed transverse loads, the first equation of equilibrium, eq. (16.50a), reduces to $\underline{N}' = 0$. Consequently, the sectional force, $\underline{N}^T = \{N_1, V_2\}$, remain constant, where N_1 and V_2 are the sectional forces along unit vectors $\bar{\imath}_1$ and $\bar{\imath}_2$, respectively. Since equilibrium must be satisfied at the tip of the beam, $N_1(\alpha_1) = N_T$ and $V_2(\alpha_1) = P_T$.

The second equation of equilibrium, eq. (16.50b), now becomes $\underline{M}' = -(\widetilde{x}_0' + \widetilde{u}')\underline{N}$, and since the sectional forces are constant, this equation integrates to $M_3(\alpha_1) = u_2 N_T - (\alpha_1 + u_1)P_T + c$, where c is an integration constant. Because the problem is two-dimensional, the other two moment components, M_1 and M_2, vanish. Imposing the moment equilibrium condition at the tip of the beam yields the integration constant and finally,

$$M_3(\alpha_1) = M_T + (L - \alpha_1 + u_1^T - u_1)P_T - (u_2^T - u_2)N_T,$$

where u_1^T and u_2^T are the beam's tip displacements along unit vectors $\bar{\imath}_1$ and $\bar{\imath}_2$, respectively.

The constitutive law for the bending moment is simply $M_3 = H_{33}\theta'$; indeed, for this two-dimensional problem, the curvature vector reduces to a single non vanishing component, $\kappa_3 = \theta'$. The constitutive laws for the sectional forces becomes

$$\begin{Bmatrix} N_T \\ P_T \end{Bmatrix} = \begin{Bmatrix} N_1 \\ V_2 \end{Bmatrix} = \underline{\underline{R}} \begin{Bmatrix} N_1^* \\ V_2^* \end{Bmatrix} = \underline{\underline{R}}\,\underline{\underline{\mathcal{C}}}^*\,\underline{\underline{R}}^T \left(\begin{Bmatrix} 1 + u_1' \\ u_2' \end{Bmatrix} - \begin{Bmatrix} C_\theta \\ S_\theta \end{Bmatrix} \right),$$

where N_1^* and V_2^* are the sectional axial and shear forces, respectively, resolved in the material system, and $\underline{\underline{\mathcal{C}}}^* = \mathrm{diag}(S, K_{22})$. Combining all the relationships obtained above yields the governing equations of the problem,

$$\begin{Bmatrix} u_1 \\ u_2 \\ \theta \end{Bmatrix}' = \begin{Bmatrix} C_\theta - 1 + \dfrac{N_T}{S}C_\theta^2 + \dfrac{N_T}{K_{22}}S_\theta^2 + (\dfrac{P_T}{S} - \dfrac{P_T}{K_{22}})S_\theta C_\theta \\ S_\theta \qquad + (\dfrac{N_T}{S} - \dfrac{N_T}{K_{22}})S_\theta C_\theta + \dfrac{P_T}{S}S_\theta^2 + \dfrac{P_T}{K_{22}}C_\theta^2 \\ \dfrac{M_T}{H_{33}} + (L - \alpha_1 + u_1^T - u_1)\dfrac{P_T}{H_{33}} - (u_2^T - u_2)\dfrac{N_T}{H_{33}} \end{Bmatrix}.$$

To better understand these equations, it is convenient to normalize all quantities. First, the material coordinate, α_1, is normalized by the length of the beam, $\eta = \alpha_1/L$, and notation $(\cdot)^+$ denotes a derivative with respect to η. The displacement components are also normalized by the beam's length, $\bar{u}_1 = u_1/L$ and $\bar{u}_2 = u_2/L$. The non-dimensional loading parameters are $\bar{N} = N_T L^2/H_{33}$, $\bar{P} = P_T L^2/H_{33}$, and $\bar{M} = M_T L/H_{33}$, and the governing equations now become

$$\begin{Bmatrix} \bar{u}_1 \\ \bar{u}_2 \\ \theta \end{Bmatrix}^+ = \begin{Bmatrix} C_\theta - 1 + \bar{N}(\bar{a}^2 C_\theta^2 + \bar{s}^2 S_\theta^2) - \bar{P}(\bar{s}^2 - \bar{a}^2) S_\theta C_\theta \\ S_\theta \quad + \bar{P}(\bar{a}^2 S_\theta^2 + \bar{s}^2 C_\theta^2) - \bar{N}(\bar{s}^2 - \bar{a}^2) S_\theta C_\theta \\ \bar{M} + \bar{P}(1 - \eta + \bar{u}_1^T - \bar{u}_1) - \bar{N}(\bar{u}_2^T - \bar{u}_2) \end{Bmatrix}, \tag{16.51}$$

where the non-dimensional stiffness properties of the beam are defined as

$$\bar{a}^2 = \frac{H_{33}}{SL^2} = \frac{1}{12}\left(\frac{h}{L}\right)^2, \quad \bar{s}^2 = \frac{H_{33}}{K_{22}L^2} = \frac{1}{10}\left(\frac{E}{G}\right)\left(\frac{h}{L}\right)^2.$$

The axial stiffness coefficient, $\bar{a}^2$, is the ratio of the bending to the axial stiffness of the beam, and the shear stiffness coefficient, $\bar{s}^2$, is the ratio of the bending to the shear stiffness of the beam. For long, slender beams, both coefficients are very small as $(h/L)^2 \to 0$ and can be assumed to vanish without noticeably affecting the predictions.

The governing equations of the problem, eqs. (16.51), take the form of three coupled first-order differential equations for the three variables of the problem, $\bar{u}_1$, $\bar{u}_2$, and θ. These equations are nonlinear due to the presence of trigonometric functions, but also because the beam's unknown tip deflections, $\bar{u}_1^T$ and $\bar{u}_2^T$, appear on the right-hand side of the equations. A convenient solution technique is to assume $\bar{u}_1^T = \bar{u}_2^T = 0$ and integrate eqs. (16.51) numerically. The solution yields an estimate of the beam's tip deflections, which are then used to obtain a refined solution by integrating eqs. (16.51) once again. An iterative procedure then yields the desired solution. This crude solution process will become unstable for large deflections of the beam. Using a relaxation factor when updating the tip deflections is often sufficient to stabilize the computation.

The deflected shape of the beam under a tip loads N_T and P_T was computed using the procedure described above. The following parameters were used: $E/G = 2.6$ and $L/h = 10$. Simulations were performed first for $\bar{N} = 0$ and $\bar{P}$ = 0.5, 1, 2, and 4. Figure 16.12 shows the predictions of the simulations. The tip deflection of the beam is not proportional to the applied load, as expected for this nonlinear problem.

A second set of simulation was performed for $\bar{P} = 4$ and $\bar{N}$ = 0, 4, 8, and 12. As the axial tip force, N_T, increases, the effective stiffness of the beam increases and the tip deflection under the constant tip transverse force decreases.

16.3.3 Extension to dynamic problems

The developments presented thus far have focused on static problems. The inertial velocity vector, $\underline{v}$, of a material point is found by taking a time derivative of its inertial position vector, eq. (16.44), to find

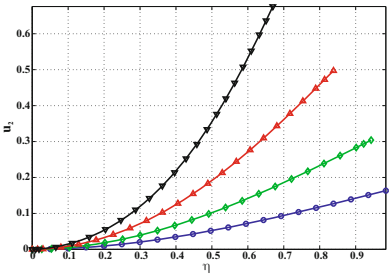

Fig. 16.12. Deflected shape of the beam under a tip transverse load for $\bar{N} = 0$. $\bar{P}$ = 0.5, 1, 2, and 4, indicated with symbols ∘, ⋄, △, and ▽, respectively.

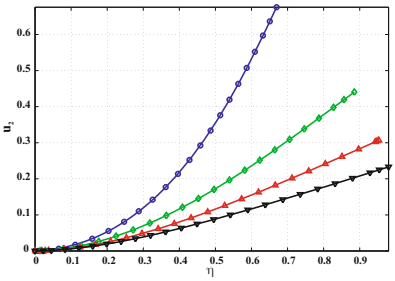

Fig. 16.13. Deflected shape of the beam under a tip transverse load for $\bar{P} = 4$. $\bar{N}$ = 0, 4, 8, and 12, indicated with symbols ∘, ⋄, △, and ▽, respectively.

$$\underline{v} = \dot{\underline{u}} + \dot{\underline{\underline{R}}}\,\underline{\underline{R}}_0\underline{s}^* = \dot{\underline{u}} + (\underline{\underline{R}}\,\underline{\underline{R}}_0)\widetilde{\omega}^*\underline{s}^* = \dot{\underline{u}} + (\underline{\underline{R}}\,\underline{\underline{R}}_0)\widetilde{s}^{*T}\underline{\omega}^*, \tag{16.52}$$

where contributions of warping of the cross-section have been ignored and $\underline{s}^{*T} = \{0, \alpha_2, \alpha_3\}$. Notation $\dot{(\cdot)}$ indicates a derivative with respect to time and $\underline{\omega}^*$ are the components of the angular velocity vector in the material system, $\underline{\omega}^* = (\underline{\underline{R}}\,\underline{\underline{R}}_0)^T\underline{\omega}$, where $\underline{\omega} = \text{axial}(\dot{\underline{\underline{R}}}\,\underline{\underline{R}})$.

The components of the inertial velocity vector of a material point resolved in the material frame now become

$$\underline{v}^* = (\underline{\underline{R}}\,\underline{\underline{R}}_0)^T\underline{v} = (\underline{\underline{R}}\,\underline{\underline{R}}_0)^T\dot{\underline{u}} + \widetilde{s}^{*T}\underline{\omega}^*. \tag{16.53}$$

The total inertial velocity of a material point has two components: the first term, $(\underline{\underline{R}}\,\underline{\underline{R}}_0)^T\dot{\underline{u}}$, due to the translation of the cross-section, and the second term, $\widetilde{s}^{*T}\underline{\omega}^*$, due to its rotation.

The kinetic energy

The kinetic energy, K, of the beam is

$$K = \frac{1}{2}\int_0^L \int_{\mathcal{A}} \rho\, \underline{v}^{*T}\underline{v}^*\, \mathrm{d}\mathcal{A}\mathrm{d}\alpha_1, \tag{16.54}$$

where ρ is the mass density of the material per unit volume of the reference configuration. Introducing eq. (16.53) for the inertial velocity yields

$$K = \frac{1}{2}\int_0^L \int_{\mathcal{A}} \rho \left[\dot{\underline{u}}^T(\underline{\underline{R}}\,\underline{\underline{R}}_0) + \underline{\omega}^{*T}\widetilde{s}^*\right]\left[(\underline{\underline{R}}\,\underline{\underline{R}}_0)^T\dot{\underline{u}} + \widetilde{s}^{*T}\underline{\omega}^*\right]\, \mathrm{d}\mathcal{A}\mathrm{d}\alpha_1. \tag{16.55}$$

The following sectional mass constants are defined

$$m = \int_{\mathcal{A}} \rho\, \mathrm{d}\mathcal{A}, \quad \underline{\eta}^* = \frac{1}{m}\int_{\mathcal{A}} \rho\, \underline{s}^*\, \mathrm{d}\mathcal{A}, \quad \underline{\underline{\varrho}}^* = \int_{\mathcal{A}} \rho\widetilde{s}^*\widetilde{s}^{*T}\, \mathrm{d}\mathcal{A}, \tag{16.56}$$

where m is the mass of the beam per unit span, $\underline{\eta}^*$ the components of the position vector of the sectional center of mass with respect to point **B**, see fig. 16.11, and $\underline{\underline{\varrho}}^*$ the components of the sectional tensor of inertia per unit span, all resolved in the material basis.

After integration over the beam's cross-section, the kinetic energy, eq. (16.55), becomes

$$\begin{aligned} K &= \frac{1}{2}\int_0^L \left[m\underline{\dot{u}}^T\underline{\dot{u}} + 2m\underline{\dot{u}}^T(\underline{\underline{R}}\,\underline{\underline{R}}_0)\,\widetilde{\underline{\eta}}^{*T}\underline{\omega}^* + \underline{\omega}^{*T}\underline{\underline{\varrho}}^*\underline{\omega}^* \right] \mathrm{d}\alpha_1 \\ &= \frac{1}{2}\int_0^L \underline{\mathcal{V}}^{*T}\underline{\underline{\mathcal{M}}}^*\underline{\mathcal{V}}^* \,\mathrm{d}\alpha_1. \end{aligned}$$

To obtain the compact form expressed by the second equality, the sectional mass matrix of the cross-section, resolved in the material basis, is defined as

$$\underline{\underline{\mathcal{M}}}^* = \begin{bmatrix} m\underline{\underline{I}} & m\widetilde{\underline{\eta}}^{*T} \\ m\widetilde{\underline{\eta}}^* & \underline{\underline{\varrho}}^* \end{bmatrix}, \tag{16.57}$$

and the sectional velocities, also resolved in the material basis, are given by

$$\underline{\mathcal{V}}^* = \begin{Bmatrix} (\underline{\underline{R}}\,\underline{\underline{R}}_0)^T\underline{\dot{u}} \\ \underline{\omega}^* \end{Bmatrix} = \begin{bmatrix} (\underline{\underline{R}}\,\underline{\underline{R}}_0)^T & \underline{\underline{0}} \\ \underline{\underline{0}} & (\underline{\underline{R}}\,\underline{\underline{R}}_0)^T \end{bmatrix} \begin{Bmatrix} \underline{\dot{u}} \\ \underline{\omega} \end{Bmatrix} = (\underline{\underline{\mathcal{R}}}\,\underline{\underline{\mathcal{R}}}_0)^T\underline{\mathcal{V}}. \tag{16.58}$$

In this expression, the sectional velocities resolved in the inertial system were defined as $\underline{\mathcal{V}}^T = \left\{\underline{\dot{u}}^T, \underline{\omega}^T\right\}$ and the following notation was introduced

$$\underline{\underline{\mathcal{R}}}\,\underline{\underline{\mathcal{R}}}_0 = \begin{bmatrix} (\underline{\underline{R}}\,\underline{\underline{R}}_0) & \underline{\underline{0}} \\ \underline{\underline{0}} & (\underline{\underline{R}}\,\underline{\underline{R}}_0) \end{bmatrix}. \tag{16.59}$$

The components of the sectional linear and angular momenta resolved in the material system, denoted $\underline{h}^*$ and $\underline{g}^*$, respectively, are

$$\underline{\mathcal{P}}^* = \begin{Bmatrix} \underline{h}^* \\ \underline{g}^* \end{Bmatrix} = \underline{\underline{\mathcal{M}}}^*\underline{\mathcal{V}}^*. \tag{16.60}$$

The governing equations

Variation of the kinetic energy is $\delta K = \int_0^L \delta\underline{\mathcal{V}}^{*T}\underline{\underline{\mathcal{M}}}^*\underline{\mathcal{V}}^* \,\mathrm{d}\alpha_1$, where the variations in velocities are $\delta[\underline{\dot{u}}^T(\underline{\underline{R}}\,\underline{\underline{R}}_0)] = (\delta\underline{\dot{u}}^T + \underline{\delta\psi}^T\,\underline{\tilde{\dot{u}}}^T)(\underline{\underline{R}}\,\underline{\underline{R}}_0)$ and $\delta\underline{\omega}^{*T} = \underline{\delta\dot{\psi}}^T(\underline{\underline{R}}\,\underline{\underline{R}}_0)$. Introducing these variations in the expression for the kinetic energy yields

$$\delta K = \int_0^L \left[(\delta\underline{\dot{u}}^T + \underline{\delta\psi}^T\,\underline{\tilde{\dot{u}}}^T)(\underline{\underline{R}}\,\underline{\underline{R}}_0)\,\underline{h}^* + \underline{\delta\dot{\psi}}^T(\underline{\underline{R}}\,\underline{\underline{R}}_0)\,\underline{g}^* \right] \mathrm{d}\alpha_1,$$

The components of the sectional linear and angular momenta, denoted $\underline{h}$ and $\underline{g}$, respectively, resolved in the inertial system are

$$\underline{\mathcal{P}} = \begin{Bmatrix} \underline{h} \\ \underline{g} \end{Bmatrix} = (\underline{\underline{\mathcal{R}}}\,\underline{\underline{\mathcal{R}}}_0)\underline{\mathcal{P}}^*, \tag{16.61}$$

where $\underline{\mathcal{P}}^*$ are the corresponding quantities resolved in the material frame, see eq. (16.60). The variation in kinetic energy finally can be written as

$$\delta K = \int_0^L (\delta\underline{\dot{u}}^T\,\underline{h} + \underline{\delta\psi}^T\,\tilde{\dot{u}}^T\,\underline{h} + \underline{\delta\dot{\psi}}^T\,\underline{g})\,\mathrm{d}\alpha_1. \tag{16.62}$$

With the help of eqs. (16.49) and (16.62), the governing equations of motion of the problem are obtained from Hamilton's principle, which states that

$$\int_{t_i}^{t_f}\int_0^L \Big\{(\delta\underline{\dot{u}}^T + \underline{\delta\psi}^T\,\tilde{\dot{u}}^T)\underline{h} + \underline{\delta\dot{\psi}}\,\underline{g} - (\delta\underline{u}'^T + \underline{\delta\psi}^T\,\widetilde{E}_1^T)\underline{N} - \underline{\delta\psi}'^T\underline{M} + \delta\underline{u}^T\underline{f} + \underline{\delta\psi}^T\underline{m}\Big\}\,\mathrm{d}\alpha_1\mathrm{d}t = 0.$$

Integration by parts yields the equations of motion of the problem

$$\underline{\dot{h}} - \underline{N}' = \underline{f}, \tag{16.63a}$$

$$\underline{\dot{g}} + \tilde{\dot{u}}\,\underline{h} - \underline{M}' - (\tilde{x}_0' + \tilde{u}')\underline{N} = \underline{m}. \tag{16.63b}$$

Example 16.3. The four-bar mechanism

Figure 16.14 depicts a flexible four bar mechanism. Bar 1 is of length 0.12 m and is connected to the ground at point **A** by means of a revolute joint. Bar 2 is of length 0.24 m and is connected to bar 1 at point **B** with a revolute joint. Finally, bar 3 is of length 0.12 m and is connected to bar 2 and the ground at points **C** and **D**, respectively, by means of two revolute joints.

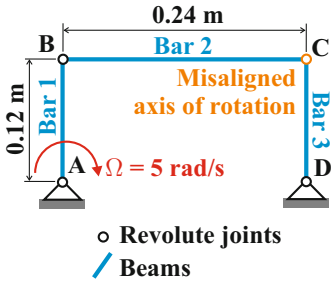

Fig. 16.14. Configuration of the four bar mechanism.

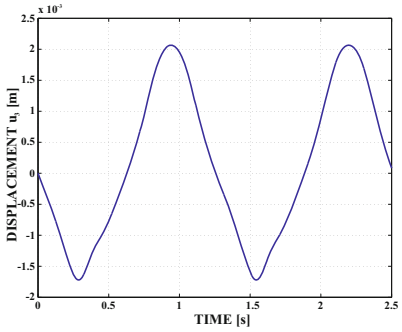

Fig. 16.15. Out-of-plane displacement u_3 at point **C**. ($\rho_\infty = 0$)

In the reference configuration, the bars of this planar mechanism intersect each other at 90 degree angles and the axes of rotation of the revolute joints at points **A**, **B**,

and **D** are normal to the plane of the mechanism. The axis of rotation of the revolute joint at point **C** is at a 5 degree angle with respect to this normal to simulate an initial defect in the mechanism. The angular velocity at point **A** of bar 1 is prescribed to be $\Omega = 5$ rad/s.

If the bars were infinitely rigid, no motion would be possible because the mechanism locks. For elastic bars, motion becomes possible, but generates large, rapidly varying internal forces. Bar 1 has the following physical characteristics: axial stiffness, $EA = 40$ MN, bending stiffnesses, $EI_{22} = EI_{33} = 2.4$ MN·m^2, torsional stiffness, $GJ = 0.28$ MN·m^2, shearing stiffnesses, $K_{22} = K_{33} = 2$ MN, mass per unit span, $m = 3.2$ kg/m, and mass moments of inertia, $m_{22} = m_{33} = 0.012$ kg·m. Bars 2 and 3 have the following physical characteristics: axial stiffness, $EA = 4$ MN, bending stiffnesses, $EI_{22} = EI_{33} = 0.24$ MN·m^2, torsional stiffness, $GJ = 0.028$ MN·m^2, shearing stiffnesses, $K_{22} = K_{33} = 0.2$ MN, mass per unit span, $m = 1.6$ kg/m, and mass moments of inertia, $m_{22} = m_{33} = 0.06$ kg·m.

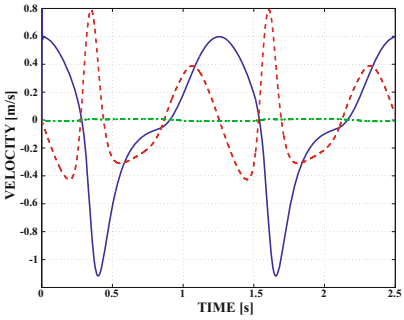

Fig. 16.16. Velocity components at point **C**. Solid line: v_1; dashed line: v_2; dashed-dotted line: v_3. ($\rho_\infty = 0$)

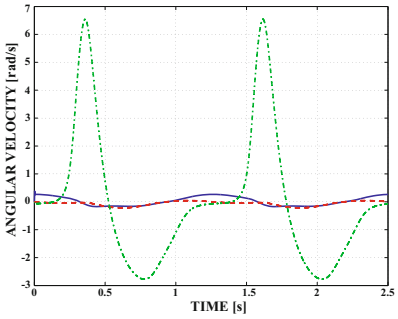

Fig. 16.17. Angular velocity components at point **C**. Solid line: ω_1; dashed line: ω_2; dashed-dotted line: ω_3. ($\rho_\infty = 0$)

This problem was simulated for a total of 2.5 s using the generalized-α scheme described in section 17.4 with $\rho_\infty = 0$; a time step of constant size $\Delta t = 2$ ms was used. If the four revolute joints had their axes of rotation orthogonal to the plane of the mechanism, the response of the system would be purely planar, and bars 1 and 3 would rotate at constant angular velocities around points **A** and **D**, respectively. The initial defect in the mechanism causes a markedly different response. Bar 1 rotates at the constant prescribed angular velocity, but bar 3 now oscillates back and forth, never completing an entire turn.

When the direction of rotation of bar 3 reverses, bar 2 undergoes large rotations, instead of near translation, and sharp increases in velocities are observed, as depicted in figs. 16.16 and 16.17, which show the three components of velocity and angular velocity at point **C**, respectively. Furthermore, fig. 16.15 depicts the time history of out-of-plane displacements at point **C**; clearly, the response of the system is three-

dimensional: the out-of-plane displacement at point **C** has a magnitude of up to about 2 mm.

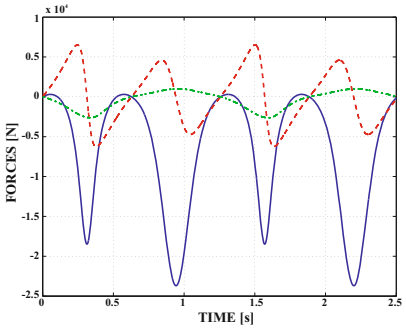

Fig. 16.18. Bar 1 force components at point **A**. Solid line: F_1; dashed line: F_2; dashed-dotted line: F_3. ($\rho_\infty = 0$)

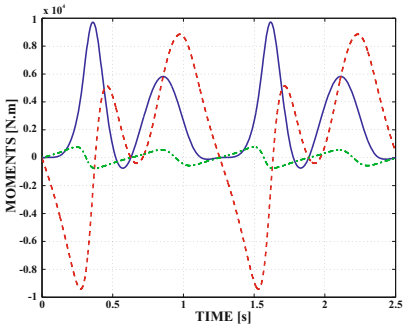

Fig. 16.19. Bar 1 moment components at point **A**. Solid line: M_1; dashed line: M_2; dashed-dotted line: M_3. ($\rho_\infty = 0$)

The time history of the three components of internal forces and bending moments in bar 1 at point **A** are shown in fig. 16.18 and 16.19, respectively. These large internal forces and moments are all caused by the initial imperfection of the mechanism.

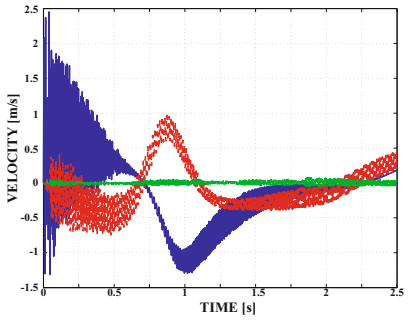

Fig. 16.20. Bar 1 force components at point **A**. Solid line: F_1; dashed line: F_2; dashed-dotted line: F_3. ($\rho_\infty = 0$)

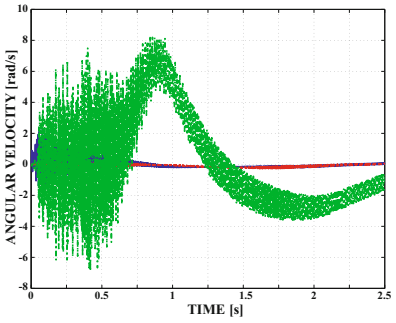

Fig. 16.21. Bar 1 moment components at point **A**. Solid line: M_1; dashed line: M_2; dashed-dotted line: M_3. ($\rho_\infty = 0$)

Next, the same simulation was run using the generalized-α scheme with $\rho_\infty = 0.85$, see eq. (17.39). In the previous simulation, the spectral radius at infinity $\rho_\infty = 0$ achieves asymptotic annihilation, see fig. 17.19; in contrast, the present simulation uses $\rho_\infty = 0.85$, which generates very little algorithmic damping, even at high frequencies. Figures 16.20 and 16.21 show the three components of velocity and angular velocity at point **C**, respectively, for $\rho_\infty = 0.85$, and should be compared with their counterparts, figs. 16.16 and 16.17, respectively, obtained for $\rho_\infty = 0$.

Using an initial time step size of $\Delta t = 2$ ms, the simulation with $\rho_\infty = 0.85$ failed to converge at time steps 10 and 14. In both cases, the time step size was halved to allow the simulation to continue. Note that very high frequency oscillations of a purely numerical origin are predicted. The asymptotic annihilation achieved for $\rho_\infty = 0$ effectively eliminates this undesirable numerical noise.

16.3.4 Problems

Problem 16.3. Conservation properties for beams
Consider an unloaded beam with linearly elastic constitutive laws. *(1)* Prove the preservation the total linear momentum of the beam. *(2)* Prove the preservation the total angular momentum of the beam. *(3)* Prove the preservation the total mechanical energy of the beam. If the beam is subjected to distributed external loads and concentrated end forces what happens to the above three preservation laws?

16.4 Formulation of plate and shell equations

Section 16.3 presents the formulation of beams, which are structures possessing one dimension that is much larger than the other two. The present section focuses on another type of structural components, plates, for which one dimension is far smaller than the other two. The mid-plane of the plate lies along the two long dimensions of the plate, and the normal to the plate extends along the shorter dimension. The term "plate" is usually reserved for flat structures, while the term "shell" refers to a curved plate.

Solid mechanics theories describing plates, more commonly referred to as *plate theories*, play an important role in structural analysis because they provide tools for the analysis of these commonly used structural components. Although more sophisticated formulations, such as three-dimensional elasticity theory, could be used for the analysis of plates and shells, the associated computational burden is often too heavy, and furthermore, plate and shell models provide valuable insight into the behavior of these structures at a much reduced computational cost. It is beyond the scope of this text to review the numerous formulations that have been developed for the analysis of plate and shell structures; comprehensive reviews of the topic are given by Noor *et al.* [317, 318].

Beam theories reduce the analysis of complex, three-dimensional structures to one-dimensional problems. Indeed, the governing equations for geometrically exact beams, eqs. (16.50), are ordinary differential equations expressed in terms of a single variable along the axis of the beam. In contrast, plate theories reduce the analysis of three-dimensional structures to two-dimensional problems. The equations of plate theory are partial differential equations in the two dimensions defining the mid-plane of the plate.

16.4.1 Kinematics of the shell problem

Figure 16.22 depicts a shell of thickness h and mid-plane surface $\mathcal{S}_m$. Let $\underline{x}_0(\alpha_1, \alpha_2)$ be the position vector of an arbitrary point **B** on the shell's mid-surface and let α_1 and α_2 be two coordinates that parameterize the mid-surface, see section 2.4.

If the mid-surface of the shell is represented by an arbitrary set of coordinates, the expressions for the first and second metric tensors of the surface, given by eqs. (2.37) and (2.47), respectively, will be complex. Consequently, it is natural to use the concept of lines of curvature introduced in section 2.4.5. In fact, shell theories are developed almost exclusively with the help of lines of curvature.

In the reference configuration frame $\mathcal{F}_0 = \left[\mathbf{B}, \mathcal{B}_0(\alpha_1, \alpha_2) = (\bar{b}_1, \bar{b}_2, \bar{b}_3)\right]$ is defined at point **B**. Vector $\bar{b}_1 = \underline{x}_{0,1} / \left\|\underline{x}_{0,1}\right\|$ and $\bar{b}_2 = \underline{x}_{0,2} / \left\|\underline{x}_{0,2}\right\|$ are unit vectors defining the plane tangent to the shell's mid-surface and unit vector $\bar{b}_3$ is the unit normal to this tangent plane. Notations $(\cdot)_{,1}$ and $(\cdot)_{,2}$ indicate derivatives with respect to α_1 and α_2, respectively. An inertial reference frame, $\mathcal{F}^I = [\mathbf{O}, \mathcal{I} = (\bar{\imath}_1, \bar{\imath}_2, \bar{\imath}_3)]$, is defined and the components of the rotation tensor that brings basis $\mathcal{I}$ to $\mathcal{B}_0$, resolved in basis $\mathcal{I}$, are denoted $\underline{\underline{R}}_0(\alpha_1)$.

The position vector of point **B** on the shell's mid-surface is denoted $\underline{x}_0(\alpha_1, \alpha_2)$. The position vector of material point **P** of the shell then becomes $\underline{x}(\alpha_1, \alpha_2, \zeta) = \underline{x}_0 + \zeta \bar{b}_3$, where ζ is the material coordinate measuring length along the normal to the mid-surface. Unit vector $\bar{b}_3$ defines a material line, *i.e.*, a set of material particles that are normal to the shell's mid-surface in the reference configuration. Coordinates α_1, α_2, and ζ form a set of curvilinear coordinates that is a natural choice of coordinates to represent the shell.

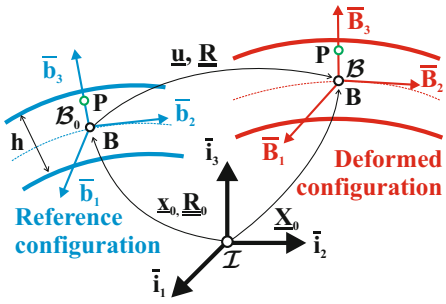

Fig. 16.22. Shell in the reference and deformed configurations.

The displacement field

In the deformed configuration, all the material points located on a normal material line of the shell move to new positions. This motion is decomposed into two parts, a rigid body motion and a warping displacement field. The rigid body motion consists of a translation of the normal material line, characterized by displacement vector $\underline{u}(\alpha_1, \alpha_2)$ of reference point **B**, and a rotation of the material line, which brings basis $\mathcal{B}_0$ to $\mathcal{B}(\alpha_1) = (\bar{B}_1, \bar{B}_2, \bar{B}_3)$, see fig. 16.22. Unit vectors $\bar{B}_1$ and $\bar{B}_2$ define the plane tangent to the deformed mid-surface of the shell and unit vector $\bar{B}_3$ is normal to this plane. The components of the rotation tensor that brings basis $\mathcal{B}_0$ to $\mathcal{B}$, resolved in basis $\mathcal{I}$, are denoted $\underline{\underline{R}}(\alpha_1, \alpha_2)$.

The warping displacement field is defined as $\underline{w}(\alpha_1, \alpha_2, \zeta) = w_1 \bar{B}_1 + w_2 \bar{B}_2 + w_3 \bar{B}_3$. This displacement field represents a warping that includes all possible deformations of the normal material line. To be uniquely defined, the warping field should be orthogonal to the rigid body motion [319, 320].

The position vector of point **P** in the deformed configuration now becomes

$$\underline{X}(\alpha_1, \alpha_2, \zeta) = \underline{X}_0 + w_1 \, \bar{B}_1 + w_2 \, \bar{B}_2 + (w_3 + \zeta) \, \bar{B}_3. \tag{16.64}$$

The position of point **B** is expressed as $\underline{X}_0(\alpha_1, \alpha_2) = \underline{x}_0 + \underline{u}$. To uniquely define the orientations of unit vectors $\bar{B}_1$ and $\bar{B}_2$, the following condition is imposed, $\bar{B}_1^T \underline{X}_{0,2} = \bar{B}_2^T \underline{X}_{0,1}$. Because $\bar{B}_i = \underline{\underline{R}} \, \bar{b}_i = (\underline{\underline{R}} \, \underline{\underline{R}}_0) \, \bar{\imath}_i$, eq. (16.64) becomes

$$\underline{X}(\alpha_1, \alpha_2, \zeta) = \underline{x}_0 + \underline{u} + (\underline{\underline{R}} \, \underline{\underline{R}}_0) \, (\underline{w} + \zeta \, \bar{\imath}_3) \, , \tag{16.65}$$

The warping displacement field is computed from the geometric and stiffness properties of the normal material line, typically by solving a one-dimensional finite element problem over the material line, as described in refs. [319, 320].

The sectional strain measures

The two-dimensional generalized strain measures for shallow shells are now defined. They are conveniently divided into three groups, the mid-surface in-plane strain components, the transverse shear strain components, and the curvature components. The mid-surface in-plane strain components are

$$e_{11} = \left(\hat{\underline{E}}_1^T \hat{\underline{E}}_1 - 1 \right) / 2, \tag{16.66a}$$

$$e_{22} = \left(\hat{\underline{E}}_2^T \hat{\underline{E}}_2 - 1 \right) / 2, \tag{16.66b}$$

$$2e_{12} = \hat{\underline{E}}_1^T \hat{\underline{E}}_2. \tag{16.66c}$$

The transverse shearing strain components are

$$2e_{13} = \hat{\underline{E}}_1^T \hat{\underline{E}}_3, \tag{16.67a}$$

$$2e_{23} = \hat{\underline{E}}_2^T \hat{\underline{E}}_3. \tag{16.67b}$$

Finally, the curvature components are

$$\kappa_{11} = \hat{\underline{E}}_1^T \frac{\hat{\underline{E}}_{3,1}}{\sqrt{a_{11}}} + \frac{1}{R_1}, \tag{16.68a}$$

$$\kappa_{22} = \hat{\underline{E}}_2^T \frac{\hat{\underline{E}}_{3,2}}{\sqrt{a_{22}}} + \frac{1}{R_2}, \tag{16.68b}$$

$$\kappa_{12} = \hat{\underline{E}}_1^T \frac{\hat{\underline{E}}_{3,2}}{\sqrt{a_{22}}} + \hat{\underline{E}}_2^T \frac{\hat{\underline{E}}_{3,1}}{\sqrt{a_{11}}}, \tag{16.68c}$$

where R_1 and R_2 are the principal radii of curvature of the shell's reference configuration as defined by eqs. (2.54).

The shell's deformation measures are defined in terms three vectors,

$$\hat{\underline{E}}_1 = \bar{b}_1 + \underline{u}_{,1}/\sqrt{a_{11}}, \tag{16.69a}$$

$$\hat{\underline{E}}_2 = \bar{b}_2 + \underline{u}_{,2}/\sqrt{a_{22}}, \tag{16.69b}$$

$$\hat{\underline{E}}_3 = \bar{B}_3, \tag{16.69c}$$

where $a_{11} = \left\|\underline{x}_{0,1}\right\|^2$ and $a_{22} = \left\|\underline{x}_{0,2}\right\|^2$ are the diagonal terms of the shell's first metric tensor in its reference configuration, see section 2.4.1 and eq. (2.37). Vector $\hat{\underline{E}}_3$ is the unit vector normal to the deformed mid-surface of the shell.

The generalized strain measures are expressed in terms of five parameters: the three components of the displacement vector, $\underline{u}$, appearing in the definition of vectors $\hat{\underline{E}}_1$ and $\hat{\underline{E}}_2$, eqs. (16.69a) and (16.69b), respectively, and the two parameters defining the orientation of the unit normal vector, $\hat{\underline{E}}_3$.

16.4.2 Governing equations

The governing equations of the problem are obtained from the principle of virtual work, which states that $\delta W_{\text{int}} + \delta W_{\text{ext}} = 0$, where δW_{int} and δW_{ext} are the virtual works done by the internal forces and externally applied loads, respectively.

Virtual work done by internal forces

For simplicity, the shell's two-dimensional generalized strain measures are collected into a single array, $\underline{e}^*$, defined as

$$\underline{e}^{*T} = \left\{e_{11}, e_{22}, e_{12}, e_{13}, e_{23}, \kappa_{11}, \kappa_{22}, \kappa_{12}\right\}.$$

The first three entries are the mid-surface in-plane strain components defined by eqs. (16.66), the next two entries the transverse shearing strain components defined by eqs. (16.67), and the last three entries the curvature components defined by eqs. (16.68).

The corresponding stress resultants are also collected in a single array, $\underline{F}^*$, defined as

$$\underline{F}^{*T} = \left\{N^*_{11}, N^*_{22}, N^*_{12}, N^*_{13}, N^*_{23}, M^*_{11}, M^*_{22}, M^*_{12}\right\}.$$

The first three entries are the in-plane forces; N^*_{11} and N^*_{22} are the stress resultants along unit vectors $\bar{B}_1$ and $\bar{B}_2$, respectively, and N^*_{12} is the in-plane shear force. The next two entries are the transverse shear forces; N^*_{13} and N^*_{23} act on faces normal to unit vectors $\bar{B}_1$ and $\bar{B}_2$, respectively. Finally, the last three entries are the bending and twisting moments. Both forces and moments are measured per unit length of the shell, and resolved in material basis $\mathcal{B}$.

Evaluating the variation of the strain components given in eqs. (16.66), (16.67), and (16.68), the virtual work done by the internal forces becomes

$$\delta W_{\text{int}} = -\int_{\mathcal{S}_m} \delta \underline{e}^{*T} \underline{F}^* \, \mathrm{d}\mathcal{S}_m = -\int_{\mathcal{S}_m} \Big\{ \delta \underline{u}_{,1}^T \underline{N}_1 + \delta \underline{u}_{,2}^T \underline{N}_2 + \delta \underline{\hat{E}}_{3,1}^T \underline{M}_1 + \delta \underline{\hat{E}}_{3,2}^T \underline{M}_2 + \delta \underline{\hat{E}}_3^T \underline{N}_3 \Big\} \, \mathrm{d}\mathcal{S}_m. \tag{16.70}$$

To simplify this expression, the following quantities were introduced

$$\underline{N}_1 = \frac{1}{\sqrt{a_{11}}} \left[N_{11}^* \underline{\hat{E}}_1 + N_{12}^* \underline{\hat{E}}_2 + N_{13}^* \underline{\hat{E}}_3 + M_{11}^* \frac{\underline{\hat{E}}_{3,1}}{\sqrt{a_{11}}} + M_{12}^* \frac{\underline{\hat{E}}_{3,2}}{\sqrt{a_{22}}} \right], \tag{16.71a}$$

$$\underline{N}_2 = \frac{1}{\sqrt{a_{22}}} \left[N_{12}^* \underline{\hat{E}}_1 + N_{22}^* \underline{\hat{E}}_2 + N_{23}^* \underline{\hat{E}}_3 + M_{12}^* \frac{\underline{\hat{E}}_{3,1}}{\sqrt{a_{11}}} + M_{22}^* \frac{\underline{\hat{E}}_{3,2}}{\sqrt{a_{22}}} \right], \tag{16.71b}$$

$$\underline{N}_3 = N_{13}^* \underline{\hat{E}}_1 + N_{23}^* \underline{\hat{E}}_2, \tag{16.71c}$$

$$\underline{M}_1 = \frac{1}{\sqrt{a_{11}}} \left[M_{11}^* \underline{\hat{E}}_1 + M_{12}^* \underline{\hat{E}}_2 \right], \tag{16.71d}$$

$$\underline{M}_2 = \frac{1}{\sqrt{a_{22}}} \left[M_{12}^* \underline{\hat{E}}_1 + M_{22}^* \underline{\hat{E}}_2 \right]. \tag{16.71e}$$

Constitutive laws

The stress resultants are related to the strain measures through the constitutive law

$$\underline{F}^* = \underline{\underline{\mathcal{C}}}^* \underline{e}^*. \tag{16.72}$$

where $\underline{\underline{\mathcal{C}}}^*$ is the shells's 8×8 sectional stiffness matrix. This matrix is a byproduct of a one-dimensional finite element analysis through the shell's thickness, as discussed in refs. [319, 320].

Virtual work done by externally applied loads

Let $\underline{f}$ and $\underline{m}$ denote the force and moment vectors applied to the shell's mid-surface per unit area, respectively. The virtual work done by these externally applied loads is expressed as

$$\delta W_{\text{ext}} = \int_{\mathcal{S}_m} \left(\delta \underline{u}^T \underline{f} + \underline{\delta \psi}^T \underline{m} \right) \, \mathrm{d}\mathcal{S}_m, \tag{16.73}$$

where $\delta \underline{u}$ is the virtual displacement vector of the point of application of the force and $\underline{\delta \psi}$ the virtual rotation vector of the same point.

Unit vector $\underline{\hat{E}}_3$ is a director, as defined in section 4.15, and can be expressed as $\underline{\hat{E}}_3 = (\underline{\underline{R}}\, \underline{\underline{R}}_0)\, \bar{\imath}_3$. A virtual change in this director's orientation then becomes $\delta \underline{\hat{E}}_3 = (\underline{\underline{R}}\, \underline{\underline{R}}_0)\, \widetilde{\bar{\imath}}_3^T \underline{\underline{b}}\, \underline{\delta \alpha}^*$, see eq. (4.113), where $\underline{\delta \alpha}^*$ is a two-parameter virtual rotation vector resolved in material basis $\mathcal{B}$ and matrix $\underline{\underline{b}}$ is defined by eq. (4.112).

The virtual work done by the applied moment becomes $\underline{\delta \psi}^T \underline{m} = \underline{\delta \psi}^{*T} \underline{m}^* = \underline{\delta \alpha}^{*T} \underline{\underline{b}}^T \underline{m}^*$, where $\underline{m}^*$ denotes the components of the applied moment vector, resolved in material basis $\mathcal{B}$, $\underline{m}^* = (\underline{\underline{R}}\, \underline{\underline{R}}_0)^T \underline{m}$. Because the last row of matrix $\underline{\underline{b}}$ stores

two vanishing entries, see eq. (4.112), the product $\underline{\underline{b}}^T \underline{m}^*$, ignores the last component of vector $\underline{m}^*$. This last component, called the *drilling moment*, is the component of the externally applied moment acting about the normal to the shell's mid-surface. Because the shell presents no stiffness about this axis, it cannot carry a drilling moment. The virtual work done by the externally applied moment, $\underline{\delta\alpha}^{*T} \underline{\underline{b}}^T \underline{m}^*$, automatically filters out the contribution of the drilling moment.

Equations of motion

Now that the virtual work done by both internal force and externally applied loads have been evaluated, the principle of virtual work states that

$$\begin{aligned} \int_{\mathcal{S}_m} \Big\{ \delta\underline{u}^T \underline{f} + \underline{\delta\alpha}^{*T} \underline{\underline{b}}^T \underline{m}^* - \delta\underline{u}^T \left[-\underline{N}_{1,1} - \underline{N}_{2,2} \right] \\ -\underline{\delta\alpha}^{*T} \underline{\underline{b}}^T \widetilde{i}_3 (\underline{\underline{R}}\,\underline{\underline{R}}_0)^T \left[\underline{N}_3 - \underline{M}_{1,1} - \underline{M}_{2,2} \right] \Big\} \, \mathrm{d}\mathcal{S}_m = 0. \end{aligned} \tag{16.74}$$

The governing equations finally become

$$\underline{N}_{1,1} + \underline{N}_{2,2} = -\underline{f}, \tag{16.75a}$$

$$\underline{\underline{b}}^T \widetilde{i}_3 (\underline{\underline{R}}\,\underline{\underline{R}}_0)^T \left(\underline{M}_{1,1} + \underline{M}_{2,2} - \underline{N}_3 \right) = -\underline{\underline{b}}^T \underline{m}^*. \tag{16.75b}$$

16.4.3 Extension to dynamic problems

The velocity of a material of the shell is computed as a time derivative of the position vector, eq. (16.65), to find $\dot{\underline{X}} = \dot{\underline{u}} + \zeta \dot{\underline{B}}_3$, where velocity components associated with the warping field have been ignored.

The kinetic energy of the shell then becomes

$$K = \frac{1}{2} \int_{\mathcal{S}_m} \int_h \rho \, (\dot{\underline{u}}^T + \zeta \dot{\underline{E}}_3^T)(\dot{\underline{u}} + \zeta \dot{\underline{E}}_3) \, \mathrm{d}\zeta \mathrm{d}\mathcal{S}_m,$$

where ρ is the material density. Integration through the shell thickness then yields

$$K = \frac{1}{2} \int_{\mathcal{S}_m} \underline{\mathcal{V}}^{*T} \underline{\underline{\mathcal{M}}}^* \underline{\mathcal{V}}^* \, \mathrm{d}\mathcal{S}_m,$$

where $\underline{\mathcal{V}}^{*T} = \left\{ \dot{\underline{u}}, \dot{\underline{B}}_3 \right\}$ is the velocity vector and the 6×6 mass matrix, $\underline{\underline{\mathcal{M}}}^*$, is defined as

$$\underline{\underline{\mathcal{M}}}^* = \begin{bmatrix} m\underline{\underline{I}} & m^* \underline{I} \\ m^* \underline{\underline{I}} & M^* \underline{\underline{I}} \end{bmatrix}.$$

The following mass coefficients were defined

$$m = \int_h \rho \, \mathrm{d}\zeta, \quad m^* = \int_h \rho\zeta \, \mathrm{d}\zeta, \quad M^* = \int_h \rho\zeta^2 \, \mathrm{d}\zeta,$$

where m is the mass of the shell per unit mid-surface area, m^*/m the location of the center mass, and M^*/m the square of the radius of gyration.

Virtual changes in the kinetic energy become

$$\delta K = \int_{\mathcal{S}_m} (\delta \underline{\dot{u}}^T \underline{h} + \delta \underline{\dot{E}}_3^T \bar{g}) \, \mathrm{d}\mathcal{S}_m, \tag{16.76}$$

where $\underline{h} = m\underline{\dot{u}} + m^* \underline{\dot{E}}_3$ and $\underline{g} = m^* \underline{\dot{u}} + M^* \underline{\dot{E}}_3$ are the linear and angular momentum vectors, respectively.

The governing equations of motion are then obtained from Hamilton's principle that becomes

$$\int_t \int_{\mathcal{S}_m} \Big\{ \delta \underline{u}^T \left[-\dot{\underline{h}} + \underline{N}_{1,1} + \underline{N}_{2,2} \right] + \underline{\delta \alpha}^{*T} \underline{\underline{b}}^T \widetilde{\imath}_3 (\underline{\underline{R}} \, \underline{\underline{R}}_0)^T$$
$$\left[-\dot{\bar{g}} - \underline{N}_3 + \underline{M}_{1,1} + \underline{M}_{2,2} \right] + \delta \underline{u}^T \underline{f} + \underline{\delta \alpha}^{*T} \underline{\underline{b}}^T \underline{m}^* \Big\} \, \mathrm{d}\mathcal{S}_m \mathrm{d}t = 0.$$

The governing equations of motion finally become

$$\dot{\underline{h}} - \underline{N}_{1,1} - \underline{N}_{2,2} = \underline{f}, \tag{16.77a}$$

$$\underline{\underline{b}}^T \widetilde{\imath}_3 (\underline{\underline{R}} \, \underline{\underline{R}}_0)^T \left[\dot{\bar{g}} + \underline{N}_3 - \underline{M}_{1,1} - \underline{M}_{2,2} \right] = \underline{\underline{b}}^T \underline{m}^*. \tag{16.77b}$$

16.4.4 Mixed interpolation of tensorial components

Several recently developed shell elements have distinguished themselves from other shell formulations because of their versatility, accuracy and robustness. One of these is the mixed interpolation of tensorial components (MITC) element developed by Bathe and his co-workers [321, 322, 323]. The MITC approach is based on the interpolation of strains at chosen sampling points (so-called "tying points"). The key issue of this approach is the selection of the tying points and corresponding interpolation functions. In case of the nine-noded MITC9 element, the interpolated strain components are defined as

$$e_{11} = \sum_\alpha g_{rr}^\alpha e_{11}^\alpha, \quad e_{22} = \sum_\alpha g_{ss}^\alpha e_{22}^\alpha, \quad e_{12} = \sum_\alpha g_{rs}^\alpha e_{12}^\alpha; \tag{16.78a}$$

$$e_{13} = \sum_\alpha g_{rr}^\alpha e_{13}^\alpha, \quad e_{23} = \sum_\alpha g_{ss}^\alpha e_{23}^\alpha. \tag{16.78b}$$

where g_{rr}^α, g_{ss}^α, and g_{rs}^α are the strain interpolation functions and e_{ij} the strain components at the α tying point, which are obtained by direct interpolation using the finite element displacement assumptions. The location of the tying points and corresponding strain interpolation functions can be found, for example, in [322, 323] for each strain component. For the MITC9 element, the strain components e_{11} and e_{13} are interpolated based on six tying points, using the shape functions g_{rr}^α. The strain components e_{22} and e_{23} are interpolated based on six tying points, using the

shape functions g^{α}_{ss}. Finally, the in-plane shearing strain component e_{12} is interpolated based on four tying points, using the shape functions g^{α}_{rs}. This approach takes care of both membrane and transverse shearing strain locking problems. The stiffness matrix of the element is then formed based on these interpolated strain components and full integration is used. The element does not present any spurious mechanism. In view of the more complicated strain interpolation and full integration scheme, the MITC9 element is a more computationally expensive element, but it is accurate and fairly insensitive to element deformations.

Example 16.4. Lateral buckling of a thin plate

Figure 16.23 depicts a thin cantilevered plate acted upon by a crank and link mechanism. The plate is of length L = 1m, height h = 80 mm, thickness t = 2 mm, and is made of steel with the following properties: Young's modulus E = 210 GPa, Poisson ratio ν = 0.25 and density ρ = 7870 kg/m^3. It is clamped along edge **AB** and a reinforcing beam is located along edge **CD**.

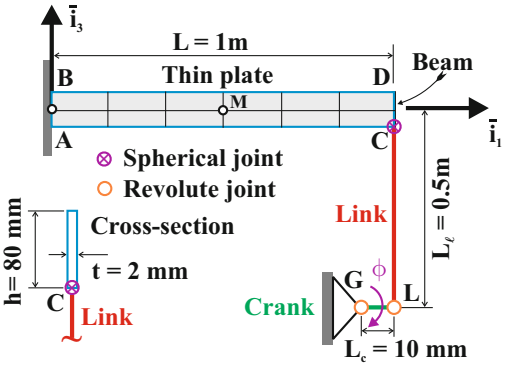

Fig. 16.23. Thin plate actuated by a crank.

At point **C**, the reinforcing beam connects to a crank and link mechanism through a spherical joint. The crank of length L_c = 10 mm is attached to the ground at point **G** and the link is of length L_ℓ = 0.5 m. The ground, crank, and link are connected together by means of revolute joints. The crank is modeled as a rigid body and its rotation is prescribed as $\phi = \pi(1 - \cos 2\pi t/T)/4$ for $t \leq T/2$ s and $\phi = \pi/2$ for $t > T/2$, where $T = 1.6$ s.

The reinforcing beam has the following physical characteristics: axial stiffness, $EA = 3.36$ MN, bending stiffnesses, $EI_{22} = EI_{33} = 4.48$ N·m^2, torsional stiffness, $GJ = 3.02$ N·m^2, shearing stiffnesses, $K_{22} = K_{33} = 1.12$ MN, mass per unit span, $m = 0.126$ kg/m, and mass moments of inertia, $m_{22} = m_{33} = 0.168$ mg·m. The link has the following physical characteristics: axial stiffness, $EA = 44$ MN, bending stiffnesses, $EI_{22} = EI_{33} = 0.3$ MN·m^2, torsional stiffness, $GJ = 28$ kN·m^2, shearing stiffnesses, $K_{22} = K_{33} = 2.4$ MN, mass per unit span, $m = 1.6$ kg/m, and mass moments of inertia, $m_{22} = m_{33} = 0.011$ kg·m.

The link is modeled as a geometrically exact beam, see section 16.3. The thin plate is modeled with a 2×6 mesh of quadratic elements. The system is simulated for 1.4 s using a constant time step $\Delta t = 0.5$ ms using the generalized-α scheme with $\rho_\infty = 0$. As the crank rotates, the plate deflects downwards then snaps laterally when its buckling load is reached. In the post-buckling regime, the plate becomes significantly softer in bending due to its large twisting allowed by the spherical joint.

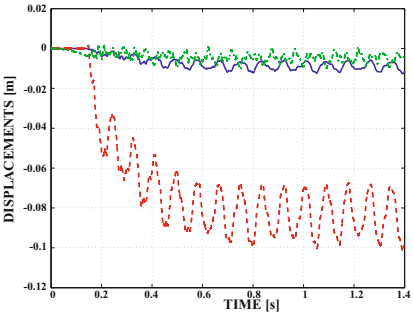

Fig. 16.24. Displacement components at point **M**. Solid line: u_1; dashed line: u_2; dashed-dotted line: u_3.

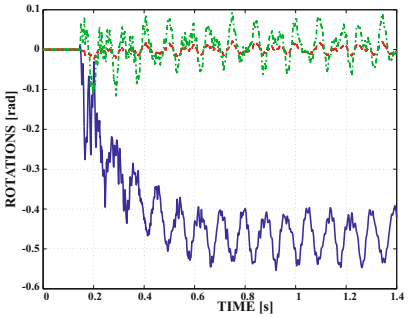

Fig. 16.25. Rotation components at point **M**. Solid line: r_1; dashed line: r_2; dashed-dotted line: r_3.

The plate's displacement components at point **M** are shown in fig. 16.24. At time $t = 0.145$ s, the plate buckles laterally and the transverse displacement, which was vanishingly small up to that time, suddenly becomes very large. For time $t > 0.8$ s, the crank angle remains constant at $\phi = \pi/2$, but the plate continues to vibrate because no dissipative mechanism is present in the system. The components of the Wiener-Milenković vectorial parameterization of rotation at point **M** are shown in fig. 16.25.

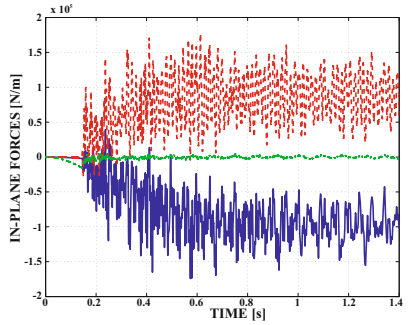

Fig. 16.26. In-plane force components at point **M**. Solid line: N^*_{11}; dashed line: N^*_{22}; dashed-dotted line: N^*_{12}.

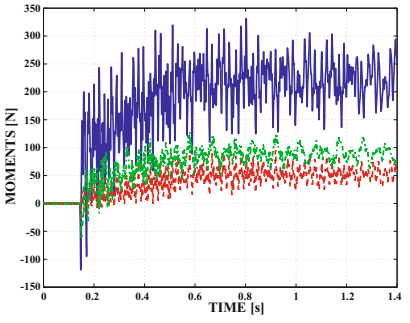

Fig. 16.27. Moment components at point **M**. Solid line: M^*_{11}; dashed line: M^*_{22}; dashed-dotted line: M^*_{12}.

The force and moments components in the plate at point **M** are depicted in figs. 16.26 and 16.27, respectively. Prior to buckling, the plate resists the bending loads applied by the driving mechanism with very little deformations. The in-plane shear force component, N_{12}^*, reflects the tip shear force applied by the crank and link mechanism, but all other force and moment components vanish. Once buckling has occurred, twisting of the plate renders it much softer in the vertical direction, offering little resistance to crank motion. Because the lateral buckling occurs so suddenly, high frequency vibrations are observed.

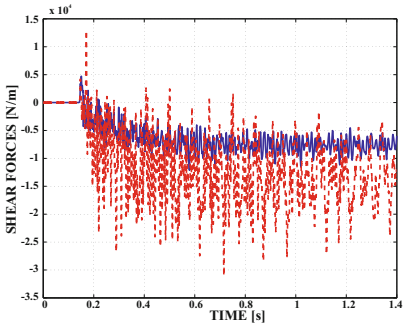

Fig. 16.28. Transverse shear force components at point **M**. Solid line: N_{13}^*; dashed line: N_{23}^*.

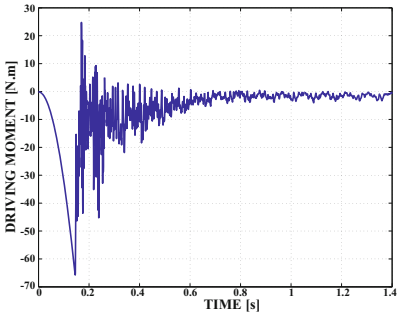

Fig. 16.29. Rotation components at midpoint. Solid line: r_1; dashed line: r_2; dashed-dotted line: r_3.

Figure 16.28 shows the corresponding transverse shear force components. Finally, the driving torque, *i.e.*, to torque applied to the crank at point **G** to achieve the prescribed schedule of angle ϕ is depicted in fig. 16.29. This quantity is, in fact, Lagrange's multiplier used to enforce the prescribed rotation holonomic constraint. As soon as the plate buckles, the magnitude if this moment decreases suddenly because of the plate's apparent softening when it buckles laterally.

Finally, the same problem was simulated using the generalized-α scheme with $\rho_\infty = 1$. In this case, due to the lack of numerical dissipation, high frequency oscillations with amplitudes an order of magnitude larger than those predicted for $\rho_\infty = 0$ are observed. This numerical noise completely obscures the results of the simulation demonstrating here again the need for integration schemes presenting numerical dissipation.